Development of the Regional Arctic System Model (RASM): Near-Surface Atmospheric Climate Sensitivity

JOHN J. CASSANO,[a,b] ALICE DUVIVIER,[a] ANDREW ROBERTS,[c] MIMI HUGHES,[a,d] MARK SEEFELDT,[a] MICHAEL BRUNKE,[e] ANTHONY CRAIG,[c] BRANDON FISEL,[f] WILLIAM GUTOWSKI,[f] JOSEPH HAMMAN,[g] MATTHEW HIGGINS,[a] WIESLAW MASLOWSKI,[c] BART NIJSSEN,[g] ROBERT OSINSKI,[h] AND XUBIN ZENG[e]

[a] *Cooperative Institute for Research in Environmental Sciences, University of Colorado Boulder, Boulder, Colorado*
[b] *Department of Atmospheric and Oceanic Sciences, University of Colorado Boulder, Boulder, Colorado*
[c] *Department of Oceanography, Naval Postgraduate School, Monterey, California*
[d] *NOAA/Earth System Research Laboratory, Boulder, Colorado*
[e] *Department of Atmospheric Sciences, University of Arizona, Tucson, Arizona*
[f] *Department of Geological and Atmospheric Sciences, Iowa State University, Ames, Iowa*
[g] *Department of Civil and Environmental Engineering, University of Washington, Seattle, Washington*
[h] *Institute of Oceanology, Sopot, Poland*

(Manuscript received 30 October 2015, in final form 14 February 2017)

ABSTRACT

The near-surface climate, including the atmosphere, ocean, sea ice, and land state and fluxes, in the initial version of the Regional Arctic System Model (RASM) are presented. The sensitivity of the RASM near-surface climate to changes in atmosphere, ocean, and sea ice parameters and physics is evaluated in four simulations. The near-surface atmospheric circulation is well simulated in all four RASM simulations but biases in surface temperature are caused by biases in downward surface radiative fluxes. Errors in radiative fluxes are due to biases in simulated clouds with different versions of RASM simulating either too much or too little cloud radiative impact over open ocean regions and all versions simulating too little cloud radiative impact over land areas. Cold surface temperature biases in the central Arctic in winter are likely due to too few or too radiatively thin clouds. The precipitation simulated by RASM is sensitive to changes in evaporation that were linked to sea surface temperature biases. Future work will explore changes in model microphysics aimed at minimizing the cloud and radiation biases identified in this work.

1. Introduction

In recent years, the high-latitude climate system has experienced pronounced changes, with the Arctic energy, moisture, carbon budgets, and atmospheric and oceanic circulation all experiencing major shifts from historical values. Perhaps most noticeable are changes seen in sea ice extent and thickness (Kwok and Rothrock 2009; Stroeve et al. 2012; Simmonds 2015).

Despite the rapid transitions seen in the Arctic and the impact of Arctic change on the global earth system, the current suite of modeling tools available to study, understand, and predict Arctic climate change is lacking (e.g., Rind 2008; Maslowski et al. 2012; Blanchard-Wrigglesworth and Bitz 2014). For example, the current generation of global climate models (GCMs) comprising phase 5 of the Coupled Model Intercomparison Project (CMIP5; Taylor et al. 2012) show large biases in atmospheric circulation, cloud–radiation interactions, and sea ice extent and thickness (e.g., Maslowski et al. 2012; Stroeve et al. 2012; Flato et al. 2013; Karlsson and Svensson 2013; Zappa et al. 2014).

Lynch et al. (1995), Giorgi (1995, 2005, 2006), and Giorgi and Gutowski (2015), and references therein, offer the history of regional climate modeling. As discussed in these and many other papers, regional models offer both advantages and disadvantages over global models. An often-cited disadvantage of regional climate models is the need to specify lateral boundary conditions (LBCs), which can be problematic if biases are present in these data. Another concern is the lack of two-way feedbacks between the simulated regional climate and the LBCs. Despite these concerns regional models offer several potential advantages. Since regional models can be run at higher resolution than global models, regional

Corresponding author: John J. Cassano, john.cassano@colorado.edu

DOI: 10.1175/JCLI-D-15-0775.1

models can explicitly represent mesoscale features that may not be resolved in global models (e.g., Maslowski et al. 2004; DuVivier and Cassano 2013) and potentially offer the ability to better resolve climate feedbacks associated with these features. The higher resolution possible in regional climate models also allows these models to serve as a test bed for future generations of global models that will eventually be run at resolutions comparable to today's high-resolution regional models. Physical parameterizations in regional models can be tailored to the specific environment of interest, thus potentially improving model performance in the area of interest without concern for deteriorating model performance in other geographical regions. Regional models often offer a wider range of parameterization options than global models, allowing for testing of a broader range of parameterizations than is possible in global models. Another potential advantage of the regional modeling framework is that the required LBCs can be controlled to assess the sensitivity of the regional climate to changes in lateral boundary conditions (e.g., Giorgi and Bi 2000; Döscher et al. 2010).

Many different regional atmospheric models have been used in the Arctic, including RCA4 (Samuelsson et al. 2011; Berg et al. 2013), CanRCM4 (Scinocca et al. 2016; Steiner et al. 2015), HIRHAM5 (Rinke and Dethloff 2000; Klaus et al. 2012; Zhou et al. 2014), CCLM (Klehmet et al. 2013; Zhou et al. 2014), and WRF Model (Hines and Bromwich 2008; Bromwich et al. 2009; Hines et al. 2011; Cassano et al. 2011; DuVivier and Cassano 2013). Over the last several years the development of Arctic system models has been suggested as one path forward for assessing Arctic change (Roberts et al. 2010; Roberts et al. 2011). Several coupled Arctic regional climate models have been developed over the past decade including HIRHAM-NAOSIM (Dorn et al. 2007, 2009, 2012), HIRHAM-HYCOM, and the Rossby Centre Atmosphere Ocean model (RCAO; Döscher et al. 2002, 2010; Koenigk et al. 2011; Döscher and Koenigk 2013).

In this paper, we introduce a new Arctic system model, the Regional Arctic System Model (RASM), and evaluate the near-surface climate in four simulations that differ in terms of ocean, sea ice, and atmospheric model options but that all use the same RASM model code. In particular, we discuss the implementation of the atmospheric component of RASM and other technical issues related to the development of RASM in section 2. In section 3 we present an analysis of the surface climate in a baseline RASM simulation and then assess the impact of changes in atmosphere and sea ice model physics on the simulated climate. In section 4, we summarize our main findings, discuss physical linkages between various model biases, and conclude with a summary of ongoing work to address the biases identified in this study.

2. Regional Arctic System Model

The Regional Arctic System Model is a limited-area, coupled atmosphere–sea ice–ocean–land model (Maslowski et al. 2012, Hamman et al. 2016). The component models of RASM include the Weather Research and Forecasting (WRF) atmospheric model, the Variable Infiltration Capacity (VIC) land and hydrology model, and regionally configured versions of the ocean and sea ice models used in the Community Earth System Model (CESM; Hurrell et al. 2013): the Los Alamos Sea Ice Model (CICE) and Parallel Ocean Program (POP). These four components are coupled using the CESM coupler (CPL7; Craig et al. 2012), with modifications important for high spatiotemporal resolution coupling (Roberts et al. 2015). RASM is run over a large pan-Arctic model domain (Fig. 1) that includes much of the Northern Hemisphere midlatitude storm track, all terrestrial drainage basins that drain to the Arctic Ocean, all sea ice–covered areas of the Northern Hemisphere, and the Arctic system domain as defined by Roberts et al. (2010).

The atmospheric model used in RASM is a modified version of the Advanced Research WRF (WRF-ARW, hereafter simply WRF) Model version 3.2 (Skamarock et al. 2008). WRF is configured on a 50-km polar stereographic grid, and this grid is shared with VIC (Fig. 1). WRF has undergone considerable development and testing for high-latitude use (e.g., Hines and Bromwich 2008; Hines et al. 2011; Cassano et al. 2011) and the version used in RASM has been optimized for use in Arctic conditions following Cassano et al. (2011) and based on additional model evaluation conducted as part of the RASM development. Despite these Arctic-specific modifications, Cassano et al. (2011) found that stand-alone WRF simulations run on the RASM domain (Fig. 1) developed significant circulation biases as a result of inadequate treatment of the model top boundary and stratosphere. To address this shortcoming, WRF in RASM applies spectral nudging above ~540 hPa with a horizontal nudging scale of ~3400 km. Further details of the WRF options used in RASM are listed in Table 1.

WRF's radiation, land, surface layer, and boundary layer schemes have been modified to facilitate coupling with POP, CICE, and VIC in RASM. The WRF radiation schemes, CAM (Collins et al. 2004) and RRTMG (Iacono et al. 2008), have been modified to export direct and diffuse visible and near-infrared solar radiation to CPL7 and import direct and diffuse visible and near-infrared albedo. The uncoupled version of WRF

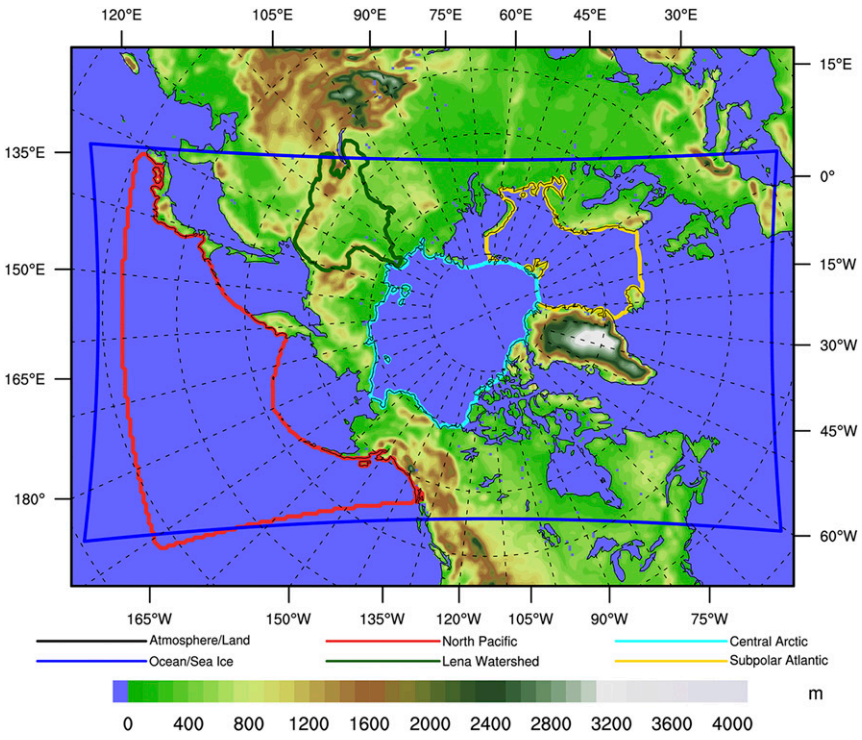

FIG. 1. RASM model domain and analysis regions (North Pacific = red outline, Lena watershed = green outline, central Arctic = light blue, and subpolar Atlantic = yellow outline). The atmosphere and land 50-km grids cover the entire map region. The extent of the ocean and sea ice 9-km grid is shown by the blue outline.

includes its own land model components, but this part of WRF has been disabled in RASM, because the VIC, POP, and CICE models supply all turbulent fluxes for the WRF surface and boundary layer schemes as well as surface albedo for the atmospheric model's radiation physics. All surface fluxes from the land, ocean, and sea ice components of RASM are provided to WRF via CPL using a 20-min coupling frequency. Compared to global

TABLE 1. List of WRF options used in the RASM_ctrl simulation.

WRF version	3.2
Horizontal grid spacing	50 km
Horizontal grid points	275 x grid points × 205 y grid points
Number of vertical levels / model top	40 / 50 hPa (lowest model level at ~12 m AGL, 10 levels in the lowest ~1 km)
Time step	WRF: 2.5 min WRF radiation: 20 min RASM coupler: 20 min
Lateral BCs	ERA-I (Dee et al. 2011)
Spectral nudging	Nudging variables: temperature and wind Nudging wavenumber: 4 (WRF x direction), 3 (WRF y direction)–(~3400 km in both the x and y directions) Nudging strength: linearly ramped up from 0 at level 20 (~540 hPa) to 0.0003 s^{-1} at level 10 (~165 hPa) Nudging depth: Applied to top 20 model levels (above ~540 hPa), with full strength in top 10 model levels (above ~165 hPa)
Longwave radiation	RRTMG (Iacono et al. 2008)
Shortwave radiation	RRTMG (Iacono et al. 2008)
Surface layer	MM5 surface layer (Paulson 1970; Dyer and Hicks 1970; Webb 1970)
Boundary layer	YSU (Hong et al. 2006)
Cloud microphysics	Morrison (Morrison et al. 2009)
Convective parameterization	Grell (Grell and Devenyi 2002)

TABLE 2. Information passed between WRF and the CPL7 coupler in RASM.

Information passed from WRF to CPL7	Information passed from CPL7 to WRF
Sea level pressure	Latent heat flux at surface
Pressure at lowest model level	Sensible heat flux at surface
Temperature at lowest model level	Temperature at 2 m
Potential temperature at lowest model level	Surface temperature
Specific humidity at lowest model level	Specific humidity at 2m
Air density at lowest model level	Log of surface roughness length
Zonal and meridional wind speed at lowest model level	Zonal and meridional surface wind stress
Downward longwave radiation flux at surface	Upward longwave radiation flux at surface
Downward direct and diffuse near-infrared (700–5000 nm) and visible (200–700 nm) solar radiation flux (four terms)	Direct and diffuse near-infrared and visible albedo (four terms)
Net shortwave radiation flux at surface	Surface snow water equivalent
Convective and large-scale liquid and frozen precipitation (four terms)	Evaporation
Height of bottom atmospheric level	Land, ocean, and ice fractions

coupled models, this is very frequent, with many recent global models exchanging ocean fluxes between all model components on time scales of several hours to one day (e.g., Gent et al. 2011; Bi et al. 2013). The purpose of RASM's frequent coupling is to minimize the response lag of the coupled system.

Information passed between WRF and the coupler in RASM (Table 2) is nearly identical to that passed between the atmospheric model and the coupler in CESM. Fluxes and state variables passed from WRF to the coupler are time-averaged over the length of the RASM coupling step (20 min), and all models in RASM are coupled at the same time interval. At land–ocean boundaries and at grid cells with both sea ice and open ocean WRF receives area-weighted sensible, latent, and momentum fluxes from VIC, CICE, and POP. Analogous to CESM, atmospheric surface stability in RASM is determined in CICE and CPL7 for the ice and ocean (Roberts et al. 2015) and in VIC for the land (Hamman et al. 2016). However, this must be consistent with surface stability used in the lowest model layer of WRF and this is done by inverting the area-weighted surface stress using the area-weighted logarithm of the surface roughness length.

The CPL7 implementation in RASM includes some important algorithmic changes to the order in which operations are performed as compared to version 1.1 of CESM. These changes enable simulation of inertial oscillations in the ice–ocean boundary layer in response to wind forcing from WRF (Roberts et al. 2015).

The ocean and sea ice component models used in RASM are version 2 of the POP ocean model (Smith et al. 1992; Dukowicz and Smith 1994; Smith et al. 2010) and version 5 of CICE (Hunke et al. 2015). POP is the same as is used in version 1.1 of CESM, but with important modifications to configure it as a regional, closed boundary model for the Arctic. POP and CICE share the same $^1/_{12}^\circ$ (~9 km) rotated sphere model grid (Fig. 1). An extended ocean domain extends beyond the inner POP/CICE domain to the edge of the RASM domain. This extended ocean domain uses climatological sea surface temperatures to provide ocean–atmosphere fluxes to WRF over the portion of the WRF domain outside of the POP/CICE domain as described in Roberts et al. (2015) and as done in other regional coupled models (Dorn et al. 2007). Further specifics of the ocean model configuration can be found in Roberts et al. (2015), except that in the current paper we utilize runoff from the VIC streamflow routing model (RVIC; Lohmann et al. 1996) as described in Hamman et al. (2016).

The version of CICE used in this paper is considerably improved from that used in CESM version 1, and is a large advance over that described for the developmental version of RASM used by Roberts et al. (2015). RASM's new baseline sea ice configuration includes anisotropic sea ice mechanics (Tsamados et al. 2013), explicit melt ponds (Hunke et al. 2013), and mushy-layer thermodynamics (Turner et al. 2013). This combined use of anisotropic dynamics, level-ice melt ponds, and mushy-layer thermodynamics within a high-resolution model represents a major step forward in fully coupled sea ice modeling. A full description and evaluation of this model configuration in RASM is currently in preparation. In this paper we address one difference between CICE version 4, with the diagnostic salinity thermodynamics of Bitz and Lipscomb (1999), and version 5, with the prognostic salinity thermodynamics of Turner et al. (2013).

The land surface component model used in RASM is the VIC model (Liang et al. 1994, 1996). VIC has been used extensively in uncoupled global and regional studies (e.g., Nijssen et al. 1997; Maurer et al. 2002; Bowling et al. 2003, 2004) and has previously been

TABLE 3. List of RASM simulations.

Simulation name	Comments
RASM_ctrl	WRF: Options as listed in Table 1 POP: Roberts et al. (2015), Hamman et al. (2016) CICE: Anisotropic rheology, Bitz–Lipscomb thermodynamics, level ice melt ponds VIC: See Hamman et al. (2016)
RASM1.0	Same as RASM_ctrl with modified ocean and ice parameters: Increased ice–ocean neutral drag coefficient from 0.00536 to 0.0067 Decreased ice–atmosphere sea ice roughness length from 0.0005 m to 0.00001842 m Increased Cf parameter that dictates how much energy is lost to friction during ridging from 17 to 34. Changed ice–ocean initial conditions from decadal spinup of coupled system to standalone ocean–ice simulation initial conditions for 1979 Decreased all CICE albedo parameters by two standard deviations (snow grain size, as well as bare ice and pond albedo) which has the effect of decreasing albedo
RASM_atm	Same as RASM_ctrl but with the following changes: Replace WRF YSU with MYNN (Nakanishi and Niino 2006) boundary layer Replace WRF Grell–Devenyi with Kain–Fritsch (Kain 2004) convective parameterization
RASM_atm_ice	Same as RASM_atm but with modified sea ice model physics Changes that significantly affected basinwide sea ice volume: Switched to mushy-layer thermodynamics from Bitz–Lipsomb thermodynamics (see also Turner and Hunke 2015). Increased Cf parameter that dictates how much energy is lost to friction during ridging from 17 to 21.3 (see also Tsamados et al. 2013). Changes to snow albedo characteristics: 1) increased the standard deviation of snow grain radius by 0.5 standard deviations; 2) decreased change in temperature per snow grain radius to 1°C from 1.5°C on sea ice; 3) decreased the maximum melting snow grain radius to 1000 from 1500×10^{-6} m [see also Urrego-Blanco et al. (2016) for an illustration of the significance of these changes in a stand-alone version of CICE] Changes that made no statistical difference to basinwide sea ice volume: Changed ice-ocean initial conditions from decadal spinup of coupled system to stand-alone ocean-ice simulation initial conditions for 1979 Set the shortwave energy absorbed by an ice algal layer to zero Changed EVP subcycling to 2 s from 10 s used in EVP and EAP Changed *e*-folding scale of ridged ice from 4 to 3 Maximum meltwater added to ponds is switched from 100% of surface runoff to 85%. The remainder runs into the ocean. Basal freezing temperature of sea ice and in the ocean model set to the liquidus temperature in mushy-layer thermodynamics, rather than being held fixed at −1.8°C.

coupled with the PSU–NCAR mesoscale model (MM5; Zhu et al. 2009). VIC has also seen significant development in its representation of cold land processes (e.g., Cherkauer et al. 2003; Bowling et al. 2003, 2004). Hamman et al. (2016) provide a detailed description of the application of VIC within RASM, including discussion on the land surface parameters and the generation of model initial conditions.

Results from four RASM simulations (Table 3), differing in ocean, sea ice, and atmospheric model options, but all using the same RASM model code, are presented below. The ERA-Interim reanalysis (ECMWF 2009; Dee et al. 2011) supplies the atmospheric LBCs and data for the WRF spectral nudging for all RASM simulations discussed in this paper, but other reanalysis or GCM datasets can be used. The closed ocean boundaries are relaxed to the Polar Science Center Hydrographic Climatology version 3.0 (PHC 3.0) (Steele et al. 2001) as described in Roberts et al. (2015). The sea ice and ocean models have been spun up from 1948 using daily CORE-2 forcing and runoff (Large and Yeager 2009), and then the model is switched into fully coupled mode in September 1979. The land surface state was spun up for a 31-yr period (January 1948–August 1979) using an uncoupled VIC only simulation forced with meteorological inputs (Hamman et al. 2016). We then run the model for an additional 10 years to allow the sea ice and snow thickness distribution to adjust to WRF coupling, which we confirm with time series of domainwide sea ice volume, snow volume, and sea surface salinity and temperature that show negligible trends or trends that are consistent with expectations over a multidecadal period.

In this paper, we analyze seasonal means for the period January 1990 through December 2014. We evaluate RASM's atmospheric simulations against ERA-Interim (ERA-I hereinafter) and top of the atmosphere (TOA) radiative fluxes observed by the CERES satellite (Loeb et al. 2009; Wielicki et al. 1996). As with all reanalyses,

ERA-I is a combination of modeled and observed fields and thus may have biases relative to the observed climate. Lindsay et al. (2014) found that ERA-I has the best performance in the Arctic when compared to similar global reanalyses, and ERA-I has similar biases in surface fields when compared to the high-resolution, regional Arctic System Reanalysis (Bromwich et al. 2016). RASM results were also compared with the Climate Forecast System Reanalysis (Saha et al. 2010) and results from this comparison were similar to those using ERA-I. Thus, we use the ERA-I dataset to evaluate the RASM-WRF simulations. For sea ice, we evaluate sea ice concentration and extent against the daily Goddard merged NOAA Climate Data Record (CDR; Meier et al. 2014) and sea ice thickness estimates from ICESat by Kwok and Cunningham (2008). Although the Arctic has undergone rapid changes during the analysis period, our primary interest here is in understanding the mean behavior of the model, and in particular the effect of different combinations of available model physics on the coupled atmospheric solution.

3. Surface atmospheric climate in RASM

a. Surface atmospheric climate in RASM1.0

In this paper we present results from four RASM simulations that differ in model physical parameterizations and parameters but that use identical model code (Table 3). The RASM_ctrl simulation was used during initial evaluation of RASM and is listed as the baseline RASM configuration in Table 3, but the first published results based on RASM are given in Hamman et al. (2016) and they used a version of RASM configured as RASM1.0 in Table 3. For consistency with this already published overview of the climate simulated by RASM we first assess the near-surface atmospheric climate of the RASM1.0 simulation.

As a result of the spectral nudging used in WRF in RASM the large-scale atmospheric circulation is relatively well simulated throughout the year with sea level pressure (SLP) biases mostly within ±4 hPa of ERA-I (Fig. 2) and the orientation and spacing of the SLP contours in RASM closely mirroring those in ERA-I. The largest biases annually are positive biases in the North Pacific (up to 4 hPa) and in the North Atlantic and Barents Sea (up to 6 hPa).

In the annual mean the RASM1.0 climate is mainly colder than ERA-I with surface temperature (Tsfc) biases of 0° to −4°C in the Atlantic and Pacific Oceans and over North America and Eurasia and biases of −2° to more than −10°C over the Arctic Ocean (Fig. 3). The cold bias over the Arctic Ocean, Eurasia, and North America is larger in winter. In summer the RASM1.0 cold bias is larger in the North Pacific, with values up to −6°C, and the winter cold land bias is replaced with a mainly warm bias of 0° to 6°C.

The RASM1.0 climate is generally drier than ERA-I with negative precipitation biases across most of the model domain for all seasons (Fig. 4). The dry bias is largest over the Pacific and Atlantic Oceans in summer and is largest over the Arctic Ocean in winter. Some areas of excess precipitation relative to ERA-I occur near the model lateral boundaries and the sharp transition between positive and negative precipitation biases in the Pacific Ocean occurs at the transition from the POP/CICE domain, where SST is predicted by RASM, to the extended ocean domain, where SST is prescribed from climatology.

Comparison of the RASM1.0 simulated downwelling longwave (LWDS; Fig. 5) and shortwave (SWDS; Fig. 6) radiation at the surface helps identify the source of the surface temperature biases discussed above. In the annual mean, RASM1.0 simulates less SWDS (biases up to $-60\,\mathrm{W\,m^{-2}}$) and more LWDS (biases up to $20\,\mathrm{W\,m^{-2}}$) over the Pacific and Atlantic Oceans compared to ERA-I. Over most land areas RASM1.0 simulates more SWDS (up to $40\,\mathrm{W\,m^{-2}}$) and less LWDS ($-20\,\mathrm{W\,m^{-2}}$) compared to ERA-I. The opposite signs of the SWDS and LWDS biases over the non-Arctic portions of the RASM domain suggest that the radiative biases in RASM1.0 are driven by errors in the simulated cloud cover, with RASM1.0 simulating too much cloud radiative impact over the oceans and too little cloud radiative impact over the land. It is important to note that the version of WRF used in RASM does not account for the radiative impact of convective clouds and thus will underestimate the cloud radiative impact in regions where convective clouds are present such as land areas in the summer and regions of oceanic stratocumulus.

Over the Arctic Ocean and adjacent land areas in Eurasia the annual mean LWDS biases are up to $-30\,\mathrm{W\,m^{-2}}$ and as large as $-50\,\mathrm{W\,m^{-2}}$ in the winter. SWDS biases over the Arctic Ocean and adjacent land areas are small in the annual and winter mean and are up to $-40\,\mathrm{W\,m^{-2}}$ in the summer. The negative SWDS bias in summer indicates that RASM1.0 is simulating too much cloud radiative impact over the Arctic in the summer whereas the large negative LWDS bias over the Arctic in the winter may be due to too little cloud cover or too optically thin clouds being simulated.

Atmospheric state biases in RASM1.0, as well as for the other three simulations listed in Table 3, generally decrease with height above the surface and become small by the midtroposphere where the WRF spectral nudging begins. Given the focus on the RASM surface climate in this paper these results are not shown here.

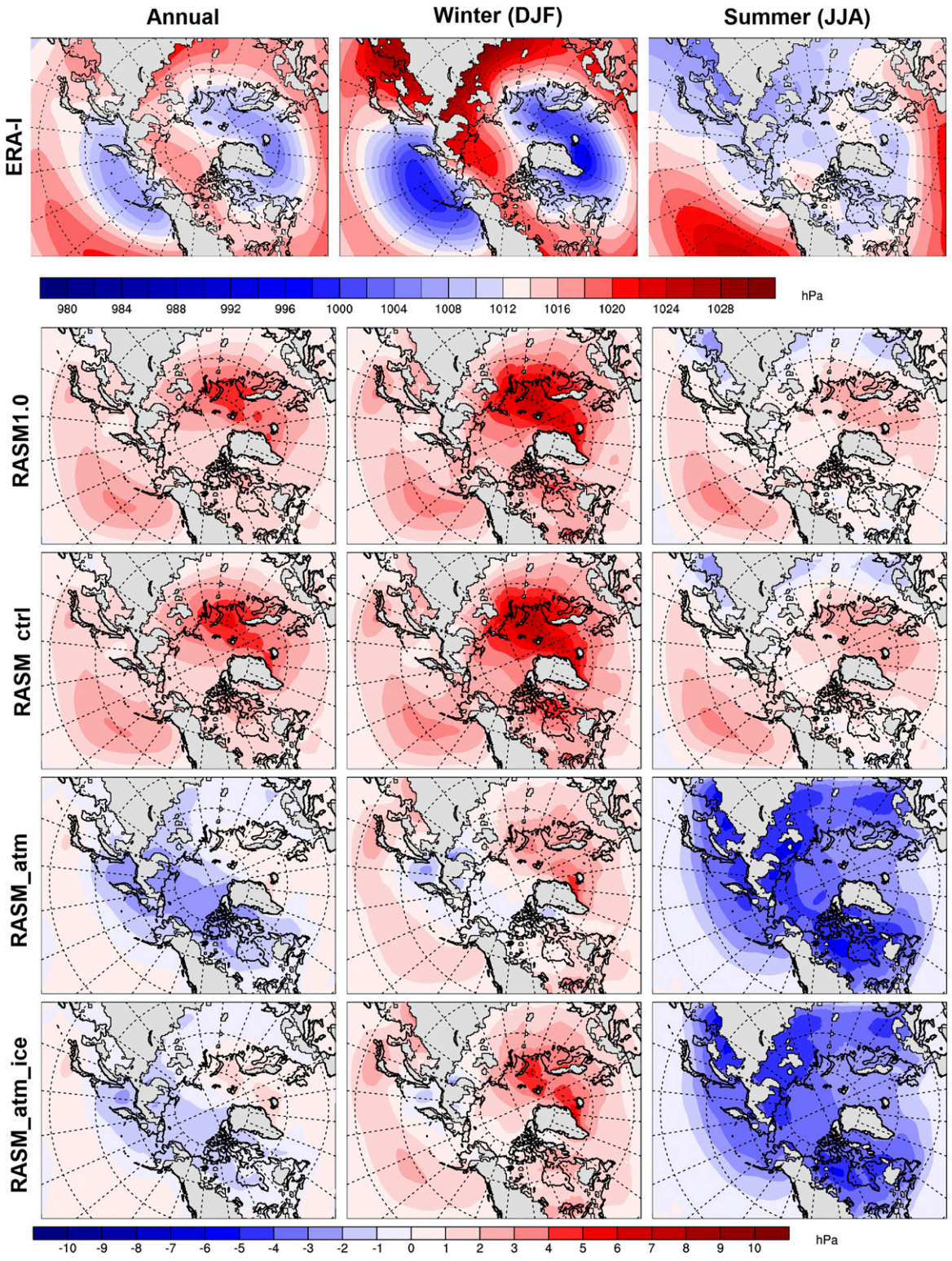

FIG. 2. (top) ERA-I (left) annual, (middle) DJF, and (right) JJA mean sea level pressure (SLP) for 1990 to 2014. Also shown are the differences between ERA-I and (second to bottom rows, respectively) RASM1.0, RASM_ctrl, RASM_atm, and RASM_atm_ice. Regions with surface elevation above 500 m are masked in gray.

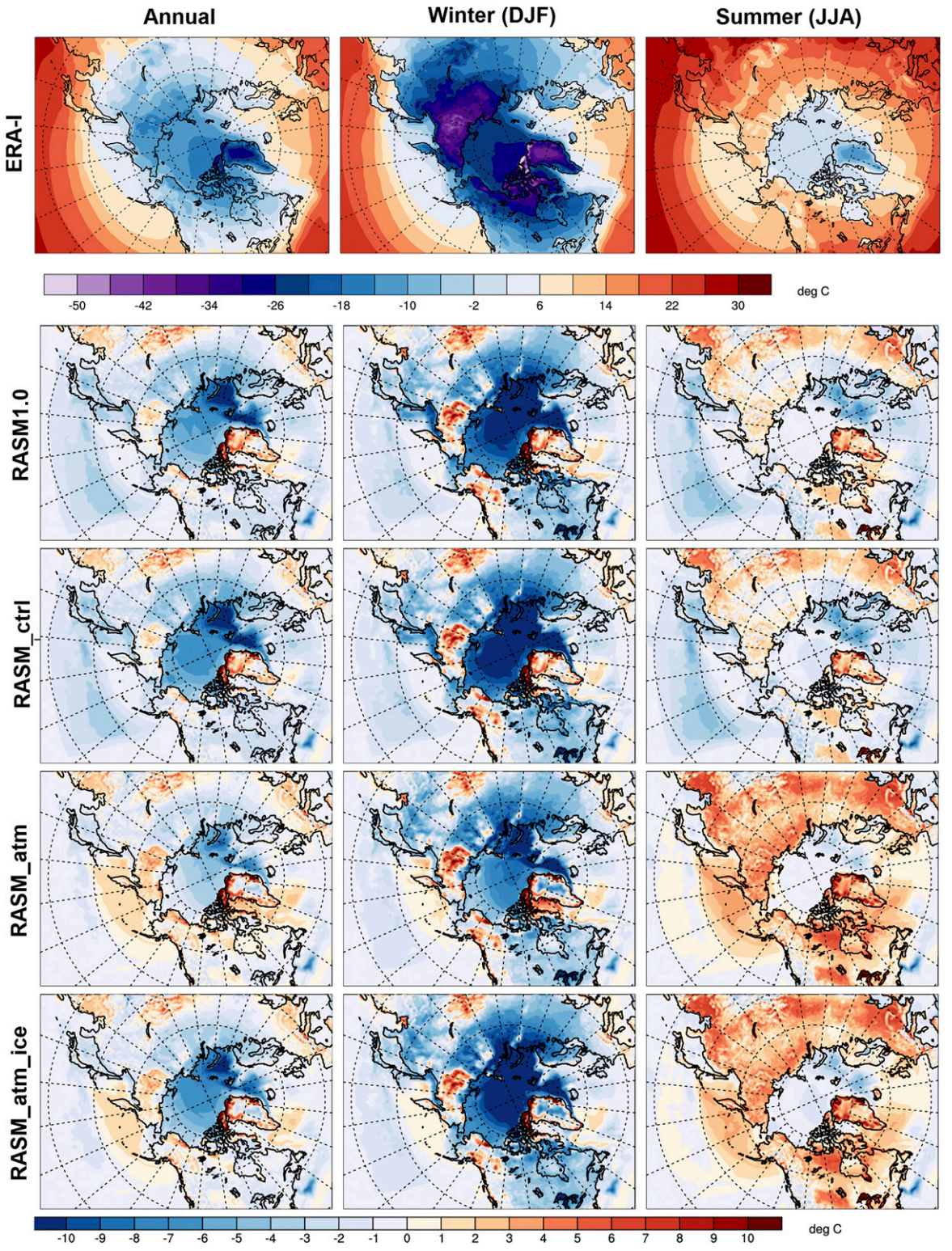

FIG. 3. (top) ERA-I (left) annual, (middle) DJF, and (right) JJA mean surface temperature (Tsfc) for 1990 to 2014. Also shown are the differences between ERA-I and (second to bottom rows, respectively) RASM1.0, RASM_ctrl, RASM_atm, and RASM_atm_ice.

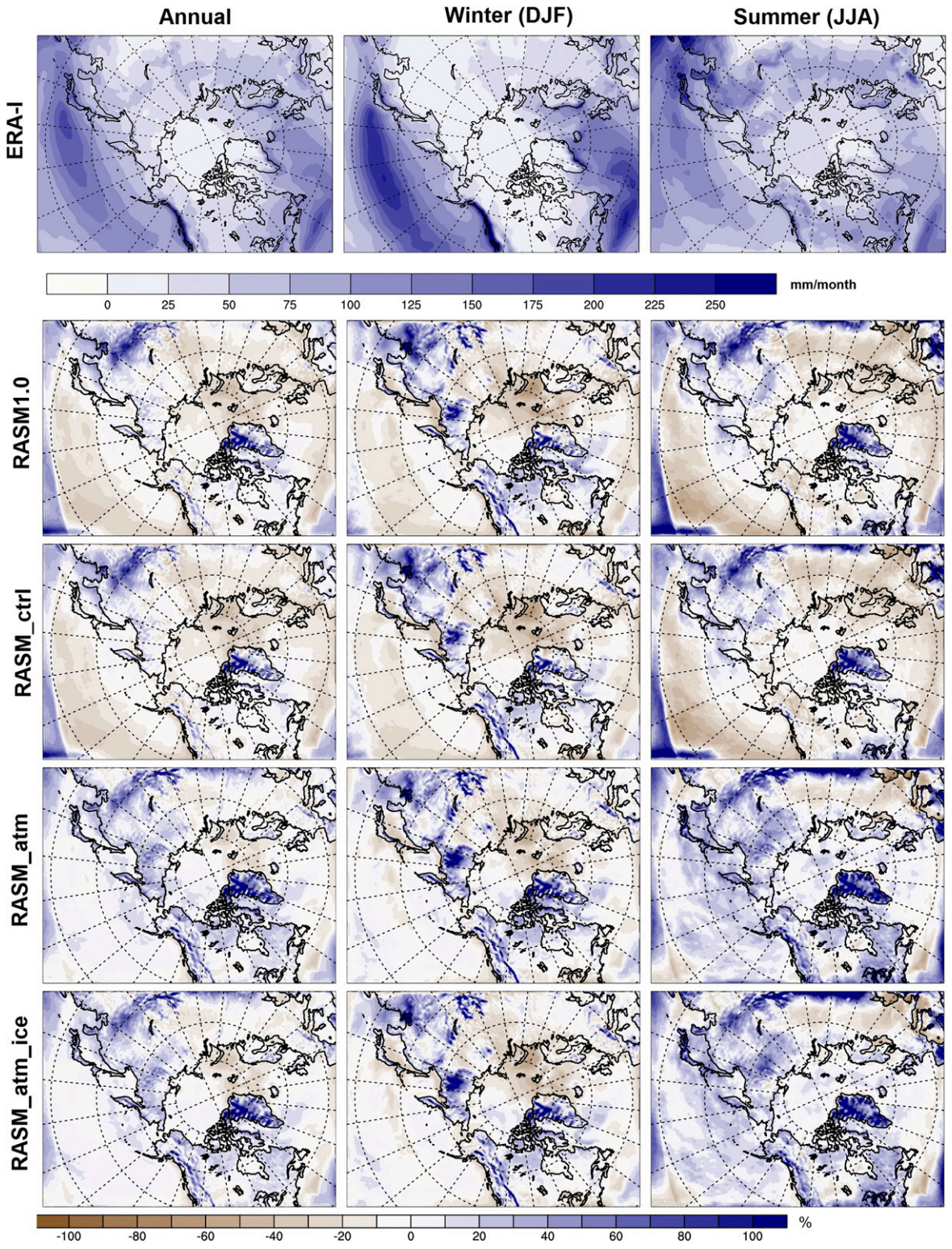

FIG. 4. (top) ERA-I (left) annual, (middle) DJF, and (right) JJA mean monthly precipitation for 1990 to 2014 (mm month^{-1}). Also shown are percent differences between ERA-I and (second to bottom rows, respectively) RASM1.0, RASM_ctrl, RASM_atm, and RASM_atm_ice.

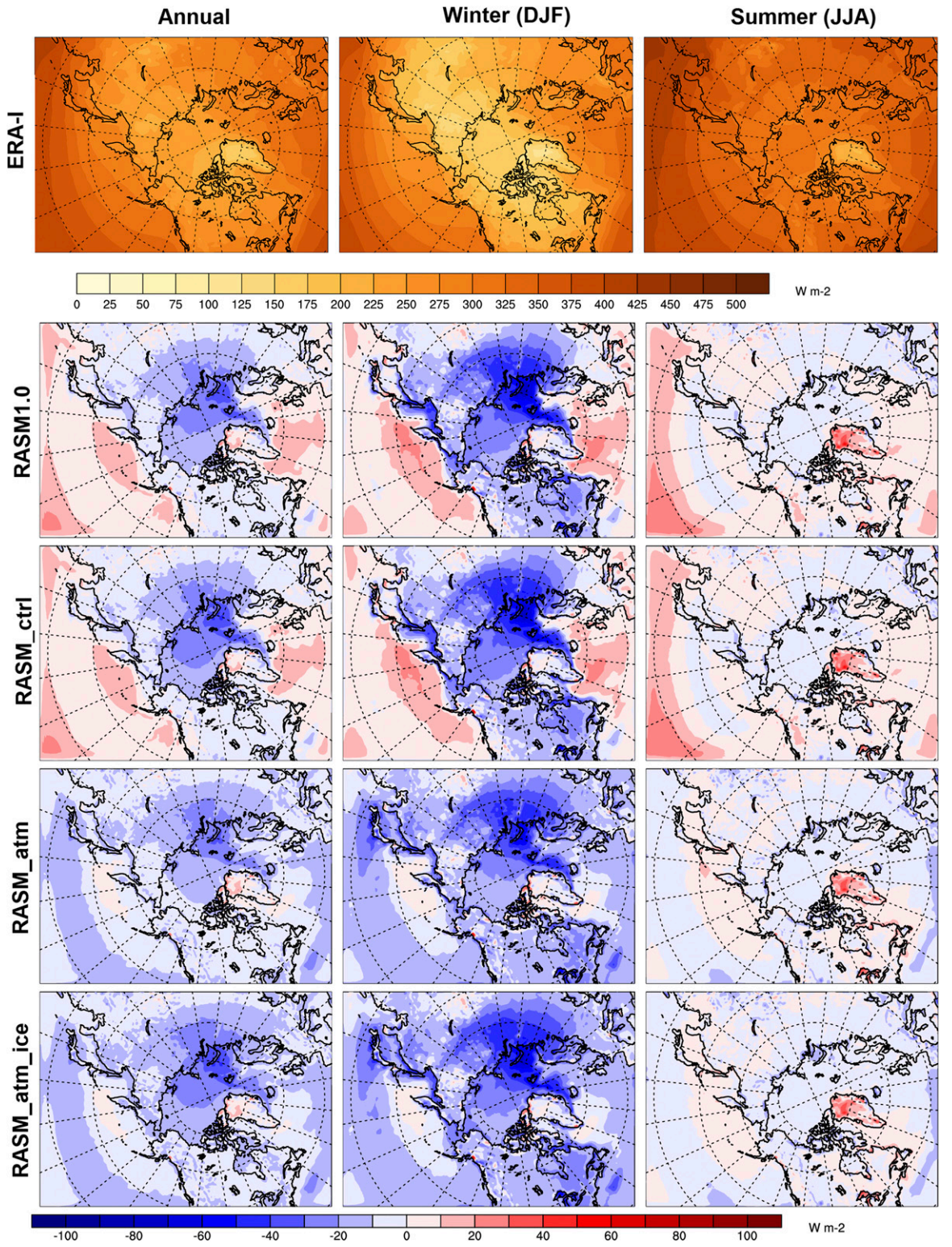

FIG. 5. (top) ERA-I (left) annual, (middle) DJF, and (right) JJA mean downward surface longwave radiation (LWDS) for 1990 to 2014. Also shown are the differences between ERA-I and (second to bottom rows, respectively) RASM1.0, RASM_ctrl, RASM_atm, and RASM_atm_ice.

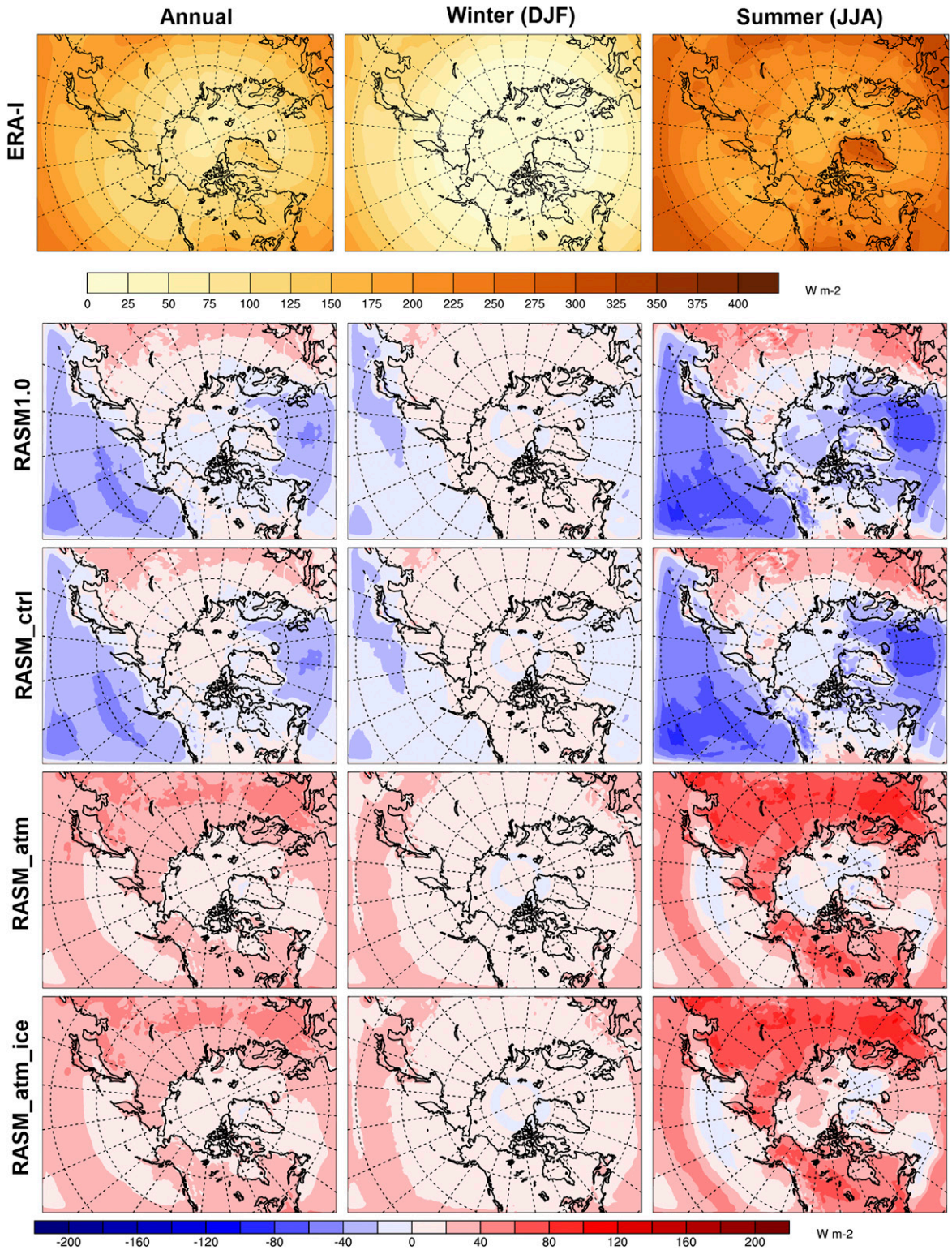

FIG. 6. As in Fig. 5, but for mean downward surface shortwave radiation (SWDS).

The surface climate biases in RASM1.0 discussed above motivated additional RASM simulations to explore if changes in RASM physics could help reduce the radiation, temperature, and precipitation biases. Results from these additional RASM simulations are discussed below.

b. *Surface atmospheric climate in alternate versions of RASM*

The RASM1.0 simulation discussed above uses modified ocean and sea ice parameters relative to the baseline version of RASM (RASM_ctrl) used for testing during the model development. The most significant model physics changes between the different RASM simulations presented in this paper were motivated to provide more physically realistic representation of climate processes rather than simply ''tuning'' the model. The RASM_atm simulation has identical model options to RASM_ctrl (Table 3) except that it uses different boundary layer [Mellor–Yamada–Nakanishi–Niino (MYNN)] and convective (Kain–Fritsch) parameterizations in WRF. These parameterization changes were based on Jousse et al. (2016), who found that WRF simulations using the MYNN boundary layer and Kain–Fritsch convective parameterizations more realistically represented boundary layer depth, and as result liquid water path and SWDS in stratocumulus clouds over the Pacific Ocean. The only model changes between the RASM_atm and RASM_atm_ice simulations are to the sea ice model physics. RASM_atm_ice incorporates more physically realistic anisotropic sea ice mechanics and sea ice thermodynamics with prognostic salinity (Table 3) and the comparison of RASM_atm and RASM_atm_ice in this manuscript represents some of the first fully coupled model results to compare these differences in sea ice model physics.

The near-surface atmospheric circulation, as represented by SLP, is reasonably well simulated in all of the RASM simulations (Fig. 2). Biases in the RASM1.0 and RASM_ctrl simulations are very similar, indicating that the differences in ocean and sea ice parameters in these simulations have little impact on the atmospheric circulation. The RASM_atm and RASM_atm_ice simulations are similar to each other, indicating little sensitivity to the sea ice changes between this pair of simulations, but simulate lower pressure than the RASM_ctrl and RASM1.0 simulations, indicating that the atmospheric physics changes impact the simulated SLP.

The Tsfc biases are similar for pairs of RASM simulations, with the RASM_ctrl and RASM1.0 simulations being similar and the RASM_atm and RASM_atm_ice simulations being similar (Fig. 3). In the annual mean the RASM_atm and RASM_atm_ice simulations are warmer than the RASM_ctrl and RASM1.0 simulations. All of the RASM simulations have a large winter cold bias in the central Arctic, with the RASM_atm simulation being 2° to 4°C warmer than the other RASM simulations in this region. The largest differences in Tsfc between the four RASM simulations occur in summer when the RASM_atm/RASM_atm_ice simulations are much warmer over land (Tsfc biases of 2° to 6°C) and open ocean (Tsfc biases of −2° to +4°C) than the RASM_ctrl/RASM1.0 simulations. The changes in the WRF physical parameterizations in the RASM_atm/RASM_atm_ice simulations have a large impact on Tsfc both over ocean and land areas but little impact in the central Arctic. The sea ice changes between the RASM_atm and RASM_atm_ice simulations have a large impact on Tsfc in the central Arctic, with the RASM_atm simulation being much warmer in this region in winter.

The RASM_ctrl and RASM1.0 simulations have similar precipitation biases; also, the RASM_atm and RASM_atm_ice simulations have similar precipitation biases (Fig. 4). The large dry bias in precipitation in the RASM_ctrl/RASM1.0 simulations is not present in the RASM_atm/RASM_atm_ice simulations. The increase in precipitation in the RASM_atm/RASM_atm_ice simulations relative to the RASM_ctrl/RASM1.0 simulations is consistent with the warmer SSTs (Fig. 3) and thus increased evaporation (not shown) over the lower latitude oceans in the RASM domain. The near step change from positive to negative precipitation bias over the Pacific Ocean at the edge of the extended ocean domain seen in the RASM1.0/RASM_ctrl simulations in the annual and summer mean is much less obvious in the RASM_atm/RASM_atm_ice simulations. This is consistent with the reduced Tsfc bias gradient in these regions in the RASM_atm/RASM_atm_ice simulations (Fig. 3) and therefore reduced evaporation gradient.

Large differences in the downwelling longwave and shortwave radiation (Figs. 5 and 6) are present between the RASM_ctrl/RASM1.0 and the RASM_atm/RASM_atm_ice simulations. In the annual, winter, and summer mean the RASM_ctrl/RASM1.0 simulations have negative SWDS biases and positive LWDS biases over the Pacific and Atlantic Ocean with opposite sign biases for these radiative fluxes over land areas. The RASM_atm/RASM_atm_ice simulations generally have positive SWDS and negative LWDS biases in all seasons over most of the model domain. For the non–Arctic Ocean portion of the model domain the opposite sign of the SWDS and LWDS biases in a given simulation suggest that the radiative biases are driven by biases in the modeled cloud cover with positive SWDS and/or negative LWDS, indicative of too few or too optically thin clouds. Based on the surface radiation biases it appears

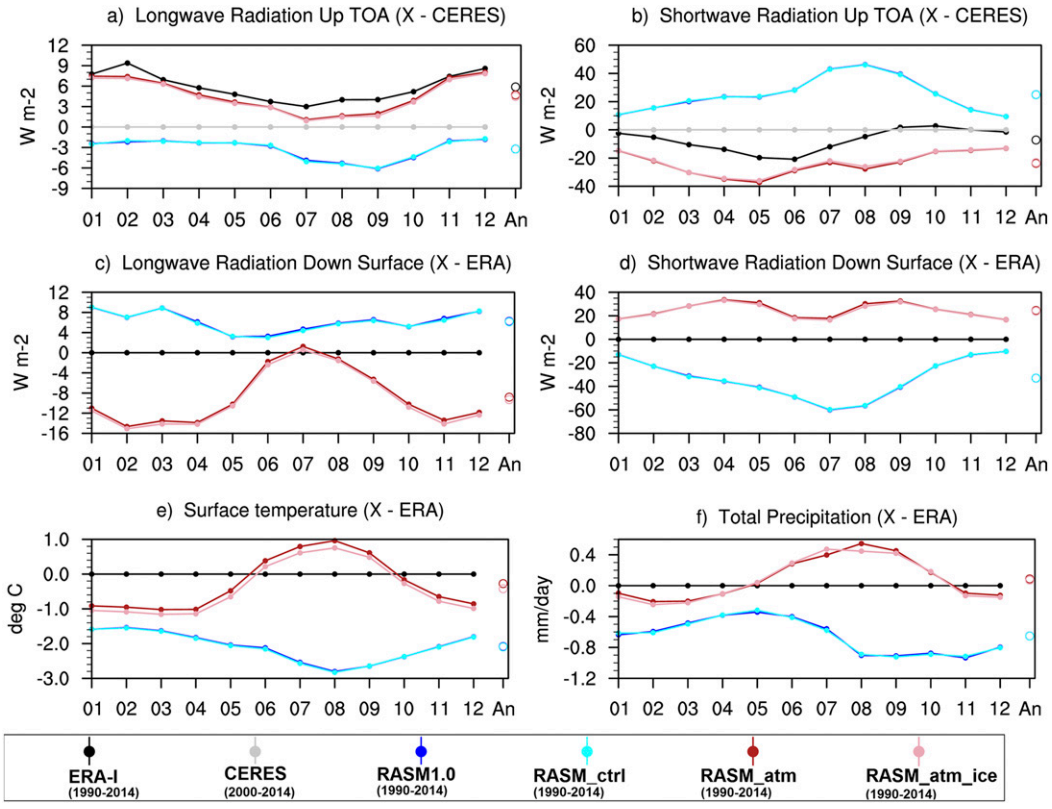

FIG. 7. Monthly and annual mean RASM1.0 (dark blue), RASM_ctrl (light blue), RASM_atm (red), and RASM_atm_ice (pink) differences from (top) CERES and (middle, bottom) ERA-I (a) upward longwave radiation at the top of the atmosphere, (b) upward shortwave radiation at the top of the atmosphere, (c) downward longwave radiation at the surface, (d) downward shortwave radiation at the surface, (e) surface temperature, and (f) total precipitation for 1990 to 2014 for the Pacific analysis domain shown in Fig. 1. Open circles on the right side of each panel show the annual mean biases for each dataset.

that the RASM_ctrl/RASM1.0 simulations are underestimating cloud radiative impact over land areas and overestimating cloud radiative impact over the Pacific and Atlantic Oceans while the RASM_atm/RASM_atm_ice simulations are underestimating cloud radiative impact across most of the model domain. Since the version of WRF used in RASM does not account for the radiative impact of convective clouds, a portion of the underestimated cloud radiative impact in all four simulations may be due to this physical inconsistency in WRF.

In the central Arctic all four RASM simulations have similar negative to near-zero LWDS biases. The negative LWDS bias in winter may be caused by RASM simulating too few or too optically thin clouds and/or the cold atmospheric bias (Fig. 3). During the summer the SWDS bias is of opposite sign in the RASM_ctrl/RASM1.0 simulations compared to the RASM_atm/RASM_atm_ice simulations and indicates too little cloud radiative impact in the RASM_atm/RASM_atm_ice simulations and too much cloud radiative impact in the RASM_ctrl/RASM1.0 simulations.

1) REGIONAL SURFACE STATE AND ENERGY BUDGET ANALYSIS

Time series of monthly mean area averages of the surface temperature, precipitation, and surface and TOA longwave and shortwave radiation are shown over different climatic regions in the RASM domain: the North Pacific (midlatitude and sub-Arctic Ocean), the Lena watershed (midlatitude and Arctic land), and the central Arctic (Fig. 1) in Figs. 7–9. This analysis provides additional information on the temporal evolution of model errors throughout the annual cycle and highlights linkages between the radiative biases, temperature, and precipitation discussed above. For this analysis the surface variables (Tsfc, precipitation, LWDS, and SWDS) simulated in RASM are compared to ERA-I while the TOA radiative fluxes (LWUT and SWUT) are compared to CERES satellite observations. The CERES estimated radiative errors at the TOA are qualitatively consistent with the ERA-I radiative errors at the surface. These figures also show the annual mean bias for all

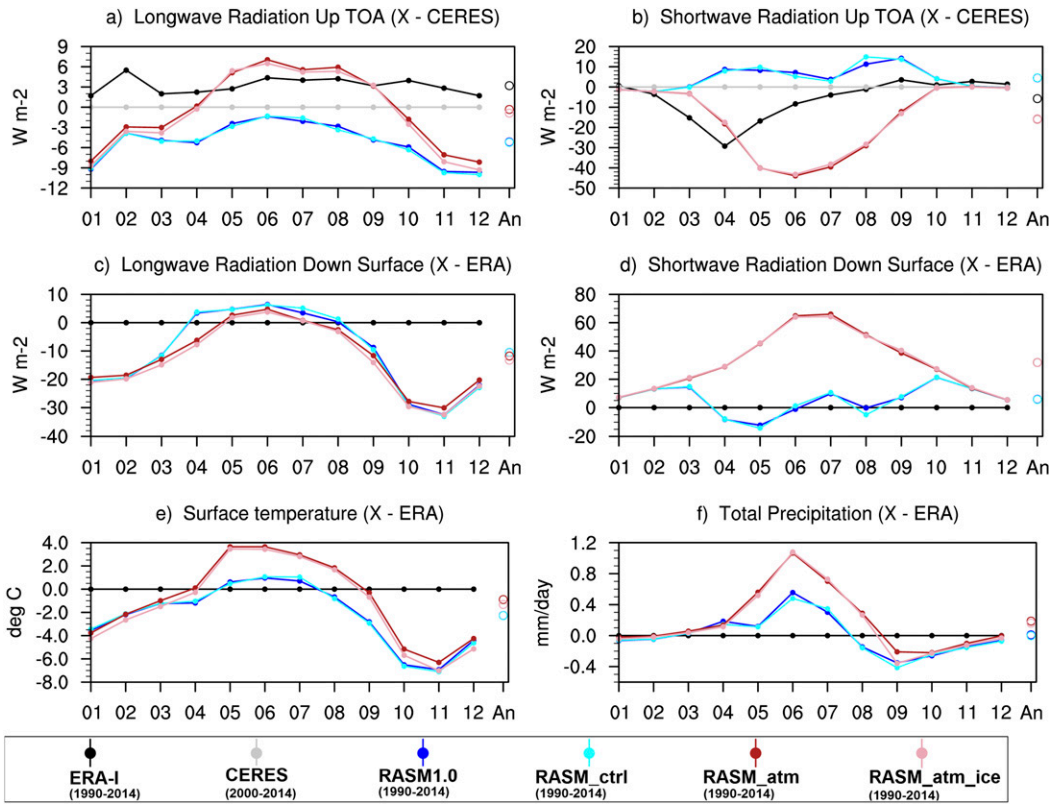

FIG. 8. As in Fig. 7, but for the Lena analysis domain shown in Fig. 1.

variables as an open circle on the right side of each figure panel.

In the North Pacific region the radiative biases at both the surface and the TOA are nearly identical for the RASM_ctrl/RASM1.0 pair of simulations and for the RASM_atm/RASM_atm_ice pair of simulations (Fig. 7). The RASM_ctrl/RASM1.0 simulations have positive SWUT biases and negative LWUT biases. The SWDS and LWDS biases are of opposite sign and range from -60 to $-10\,\mathrm{W\,m^{-2}}$ for SWDS and 4 to $10\,\mathrm{W\,m^{-2}}$ for LWDS. The sign of these biases are consistent with RASM_ctrl/RASM1.0 simulating too many clouds or overly optically thick clouds over the North Pacific throughout the annual cycle. The overall negative radiation bias at the surface results in a cold SST bias throughout the year, with the largest radiation and Tsfc biases in July and August. The cold SST bias results in a negative evaporation bias relative to ERA-I (not shown) and a negative precipitation bias across this region.

In the North Pacific region the RASM_atm/RASM_atm_ice simulations have opposite sign radiative biases compared to the RASM_ctrl/RASM1.0 simulations (Fig. 7). The RASM_atm/RASM_atm_ice simulations have smaller magnitude shortwave radiation biases (15 to $35\,\mathrm{W\,m^{-2}}$) than the RASM_ctrl/RASM1.0 simulations but slightly larger magnitude longwave radiation biases. The shortwave and longwave biases are generally opposite in sign and are consistent with this pair of RASM simulations simulating too little cloud radiative impact over the North Pacific. This is consistent with the results in Jousse et al. (2016) that found that the combination of MYNN boundary layer and Kain–Fritsch convective parameterization reduced the cloud water path over the North Pacific resulting in increased SWDS. In response to the positive surface radiation bias these simulations have positive SST biases from June to September and negative biases during the winter and early spring. The precipitation biases mirror the SST biases. These results indicate that in the North Pacific the change in WRF model physics alters the sign of the cloud, and thus radiation, biases in RASM with little sensitivity evident for changes in ocean or ice model parameters (RASM1.0 compared to RASM_ctrl) or for changes in ice model processes (RASM_atm compared to RASM_atm_ice). The sea surface temperature and precipitation respond to the surface radiative bias with the excess cloud cover simulations (RASM1.0 and RASM_ctrl) having negative surface radiation, SST, and precipitation biases and the reduced cloud cover simulations (RASM_atm and

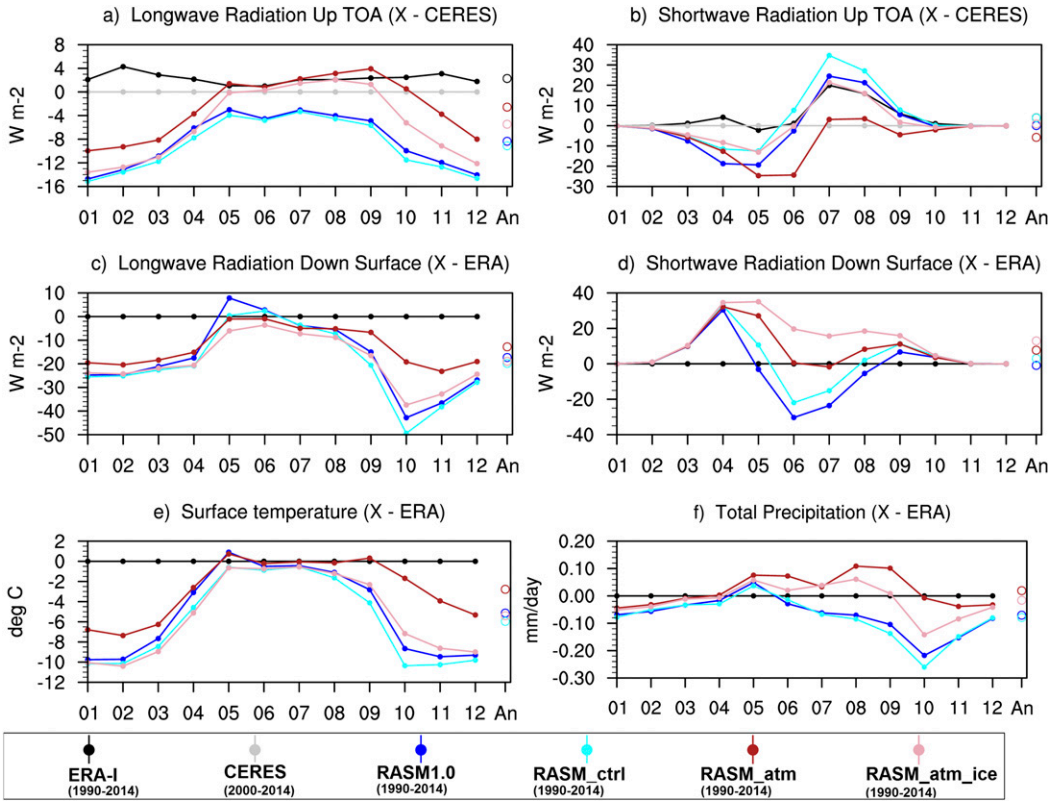

FIG. 9. As in Fig. 7, but for the central Arctic analysis domain shown in Fig. 1.

RASM_atm_ice) having positive surface radiation, SST, and precipitation biases during the summer.

The regional model biases in the Lena watershed (Fig. 8) are representative of the model biases across much of Eurasia and North America. Similar to the results for the North Pacific region the RASM_ctrl and RASM1.0 pair of simulations have similar biases, and the RASM_atm and RASM_atm_ice pair of simulations have similar biases for the TOA and surface radiative fluxes, Tsfc, and precipitation. The RASM_ctrl/RASM1.0 simulations have smaller magnitude SWUT and SWDS biases than the RASM_atm/RASM_atm_ice simulations, which are as large as 60 $W m^{-2}$ for SWDS. The shortwave radiation biases indicate a significant underestimation of clouds over the Lena watershed in the RASM_atm/RASM_atm_ice simulations, especially in summer, and a relatively good cloud simulation in the RASM_ctrl/RASM1.0 pair of simulations. For the Lena watershed all four RASM simulations have similar LWDS biases throughout the year.

Over the Lena watershed all four simulations have similar cold Tsfc biases from October through April that mirror the negative LWDS bias. In summer the RASM_atm/RASM_atm_ice simulations are much warmer than the RASM_ctrl/RASM1.0 simulations. Hamman et al. (2016) note that at high latitudes in North America and eastern Siberia the retreat of snow-covered area in RASM1.0 precedes satellite observations by about 15 days. This early retreat of the snow cover in April and May, which is more rapid in the RASM_atm/RASM_atm_ice simulations and is driven by the increasing positive SWDS bias in these simulations, contributes to the early summer warm bias in May and June, whereas the large positive SWDS bias later in the summer sustains the warm Tsfc bias, most noticeably in the RASM_atm/RASM_atm_ice simulations.

The precipitation bias in the Lena region is similar for all four simulations from September through April. All four simulations have positive summer precipitation biases that peak in June but the biases in the RASM_atm/RASM_atm_ice simulations are more than twice as large as those in the RASM_ctrl/RASM1.0 simulations. The increased precipitation in the RASM_atm/RASM_atm_ice simulations may be a response to the increased oceanic evaporation as a result of the warmer SSTs compared to the RASM_ctrl/RASM1.0 pair of simulations (Fig. 3 and 7) or due to increased evaporation and convection due to the increased surface temperature over land in these simulations.

In the central Arctic in the spring (Fig. 9) all four RASM simulations overestimate SWDS. The RASM_atm_ice

simulation has the largest SWDS bias, and this positive SWDS bias persists throughout the summer and early fall. The RASM_atm simulation SWDS bias drops to near zero in midsummer and then becomes slightly positive for late summer and early fall. The RASM_ctrl/RASM1.0 simulations have negative SWDS biases from June through August and slight positive SWDS biases in September and October. The sign of the shortwave biases indicates too little cloud radiative impact in spring and early summer and again in fall for all four simulations. The RASM_atm/RASM_atm_ice pair of simulations maintain this negative cloud bias throughout the summer whereas the RASM_ctrl/RASM1.0 simulations have too much cloud radiative impact in midsummer.

The longwave biases in the central Arctic are similar for all four RASM simulations with the largest negative LWUT and LWDS (up to $-50\,\mathrm{W\,m^{-2}}$) biases from late fall through winter. The RASM_atm simulation has the least negative longwave bias of all four simulations. From May through September the LWDS biases are near $0\,\mathrm{W\,m^{-2}}$ in all four RASM simulations. The negative wintertime longwave biases may be caused by too few clouds or too optically thin clouds (Shupe and Intrieri 2004; Bennartz et al. 2013; Miller et al. 2015), consistent with previous high-latitude studies with different configurations of WRF that have shown that WRF radiative biases are largely driven by cloud biases (Bromwich et al. 2016; Porter et al. 2011; Hines et al. 2011; Bromwich et al. 2009). It is also possible that the negative longwave biases may reflect the cold and/or dry bias in the atmosphere, resulting in an optically thinner atmosphere.

All four RASM simulations have a cold Tsfc bias in the central Arctic from October through April and then a near-zero Tsfc bias from May through September. The RASM_atm simulation has the smallest cold bias of all four RASM simulations. The cold bias in most of these simulations develops quickly in September and October whereas the cold bias develops more slowly in the RASM_atm simulation. It is unclear whether the cold Tsfc winter bias is driven by the negative LWDS bias discussed above or if the cold bias, both at the surface and in the lower atmosphere (not shown), is driving the negative LWDS and LWUT biases. The larger cold bias in the RASM_atm_ice simulation compared to the RASM_atm simulation indicates that the changes in the sea ice model physics between this pair of simulations (Table 3) are impacting the near-surface atmospheric state. The switch from diagnostic (Bitz–Lipscomb thermodynamics) to prognostic (mushy-layer thermodynamics) sea ice salinity results in thicker sea ice, consistent with stand-alone sea ice model results of Turner and Hunke (2015), and is likely the main factor that contributes to the colder Tsfc in the RASM_atm_ice simulation.

The RASM_atm/RASM_atm_ice simulations have a negative precipitation bias from October through April and a positive precipitation bias from May through September. The RASM_ctrl/RASM1.0 simulations are drier than the RASM_atm/RASM_atm_ice simulations, consistent with results from the North Pacific and Lena watershed discussed above.

2) Sea ice in RASM simulations

All four RASM simulations have negative sea ice concentration biases in the central Arctic in summer, and excessive sea ice cover in the Barents, Kara, and Greenland Seas (Fig. 10). Within the central Arctic, the largest negative bias occurs in RASM_atm. The statistical significance of the bias is based upon Welch's two-sided t test using lag-1 autocorrelation to estimate effective sample size following von Storch and Zwiers (1999) and Wilks (2006).

Differences in sea ice thickness between the RASM simulations and ICESat more clearly indicate the sensitivity of the simulated sea ice state to changes in RASM configuration (Figs. 11 and 12). The comparisons in Figs. 11 and 12 should only be considered as approximate, due to uncertainties in sea ice density (Tilling et al. 2015) and a small inconsistency in the periods represented by RASM 2-monthly means and ICESat retrievals for each 2-month window. However, the bias estimate provided here is sufficient for indicating broad limitations of and differences between each of the four RASM model runs.

Figures 11 and 12 indicate that RASM_ctrl/RASM1.0 simulations have the largest positive ice thickness bias of the four RASM simulations. The RASM_atm/RASM_atm_ice simulations have thinner ice, more compatible with the Kwok and Cunningham (2008) ice thickness estimates, with the RASM_atm simulation having the largest negative ice thickness biases. These results indicate that the sea ice responds to changes in the WRF physics with a large decrease in ice thickness between the RASM_ctrl and RASM_atm simulations. For simulations with the same WRF physics the sea ice thickness responds to both changes in ice and ocean parameters (RASM_ctrl compared to RASM1.0) and to changes in sea ice model physics (RASM_atm compared to RASM_atm_ice).

Perhaps most important in the sea ice comparison between RASM_atm and RASM_atm_ice is that without mushy-layer thermodynamics (RASM_atm) in CICE, there is a seasonal inconsistency in the thickness bias. Although there are several other differences

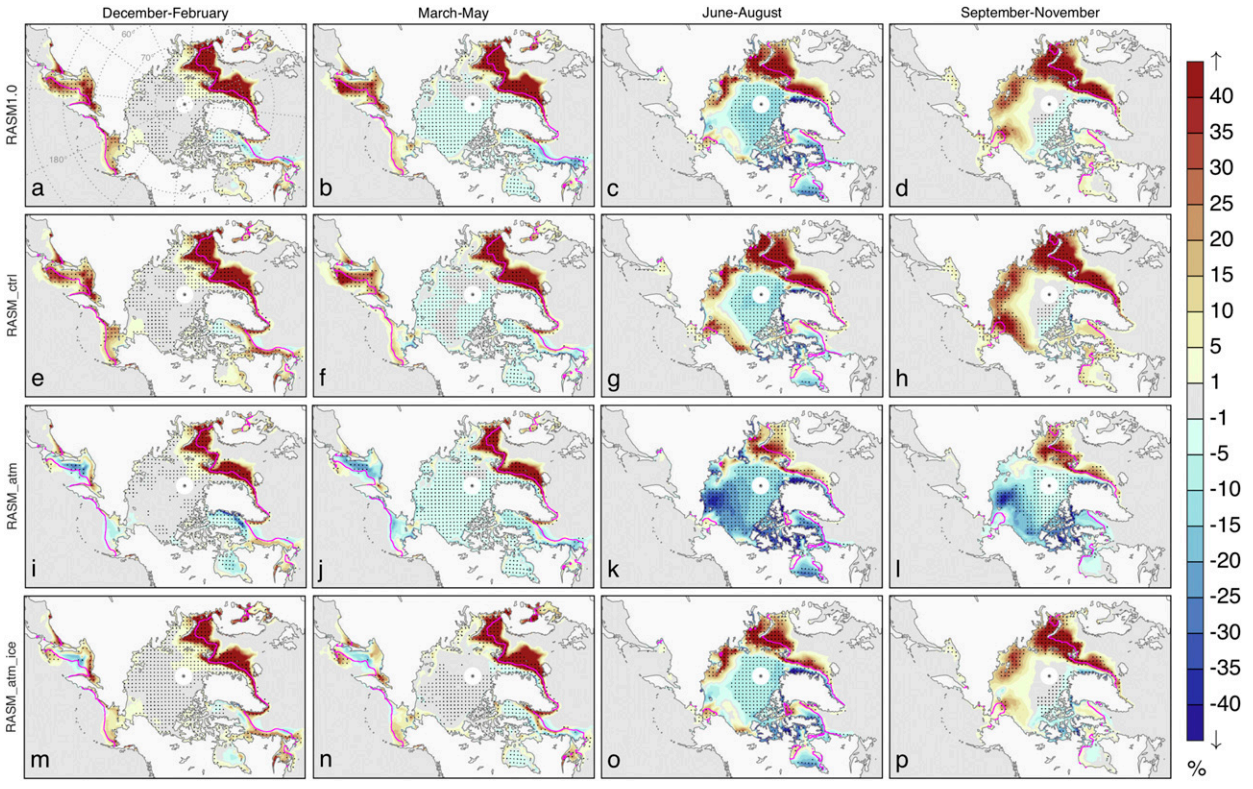

FIG. 10. Difference from NOAA CDR interpolated sea ice concentration for (a)–(d) RASM1.0, (e)–(h) RASM_ctrl, (i)–(l) RASM_atm, and (m)–(p) RASM_atm_ice sea ice concentration for (left to right) DJF, MAM, JJA, and SON. The time series is analyzed from December 1989 through to November 2014. The magenta contour indicates NOAA CDR mean 15% sea ice extent, and stippling indicates difference at the 99% confidence interval.

between RASM_atm and RASM_atm_ice, the change in thermodynamics is the largest physics change (Table 3). This result suggest that use of prognostic salinity better simulates the annual thickness cycle of sea ice in the central Arctic, and warrants further investigation in a follow-on investigation. Overall, the RASM_atm_ice simulation produces the most realistic sea ice state of the four RASM simulations considered here in terms of central Arctic thickness, but it still overestimates sea ice extent on the Atlantic side of the Arctic (Fig. 10).

The source of the persistent positive sea ice bias on the Atlantic side of the Arctic is the subject of ongoing investigations. One possible explanation would be errors in oceanic heat transport into this region, but heat fluxes across the Barents Sea opening simulated in RASM are similar to observational estimates, suggesting that oceanic processes are not a major factor in this regional sea ice bias. This region was shown to have the largest atmospheric cold bias and largest negative LWDS biases (Figs. 3 and 6) in the RASM domain but these atmospheric biases may either be a response to the excess sea ice or may be forcing the excess sea ice. The surface radiation, Tsfc, and precipitation biases for the subpolar Atlantic region (Fig. 13) are similar to those shown for the central Arctic (Fig. 9). In the subpolar Atlantic region the RASM_atm/RASM_atm_ice simulations have a positive SWDS bias throughout the summer while the RASM_ctrl/RASM1.0 simulations have a negative SWDS bias. All four simulations have near-zero LWDS biases during the summer. The larger amount of SWDS in the RASM_atm/RASM_atm_ice simulations in summer reduces the positive sea ice extent bias slightly (Fig. 10). All four simulations have large negative LWDS biases in the subpolar Atlantic from October through April of up to $-40\,\mathrm{W\,m^{-2}}$.

4. Discussion and conclusions

In this paper we have presented an assessment of the near-surface atmospheric climate in the initial version of the Regional Arctic System Model (RASM), comparing four RASM simulations that differ in terms of ocean and sea ice model parameters and atmosphere and sea ice physics (Table 3) but that all use the same model code. All four simulations simulate the near-surface circulation, as depicted by SLP (Fig. 2), relatively well. The

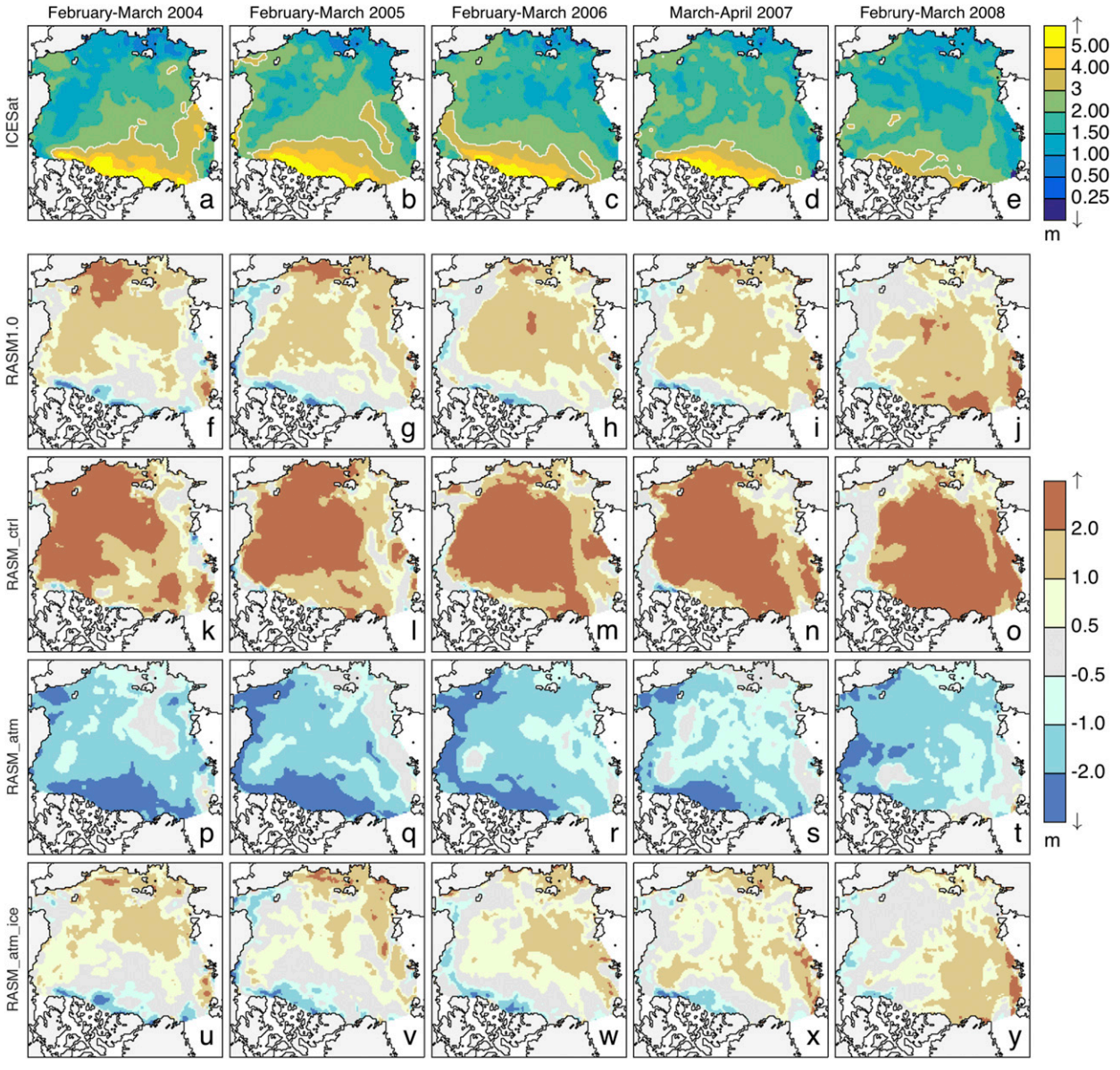

FIG. 11. (a)–(e) Spring (February–March) sea ice thickness estimated from ICESat, and mean deviation from Kwok and Cunningham (2008) for (f)–(j) RASM1.0, (k)–(o) RASM_ctrl, (p)–(t) RASM_atm, and (u)–(y) RASM_atm_ice.

RASM_ctrl/RASM1.0 simulations tend to have cold Tsfc biases over the Pacific and Atlantic Oceans and a slight warm bias over land in summer. The RASM_atm/RASM_atm_ice simulations have smaller ocean Tsfc biases but a larger warm bias over land in summer. All four simulations have a large cold bias in the central Arctic and over adjacent high-latitude land areas in winter (Fig. 3). The differing magnitudes of the land and ocean temperature biases in these simulations suggest that different model configurations may be most appropriate depending on the intended application of RASM.

All of the temperature biases are shown to be related to biases in downward surface radiative fluxes (Figs. 5 and 6) associated with errors in the simulated cloud cover in RASM. The RASM_ctrl/RASM1.0 simulations simulate too much oceanic cloud radiative impact and thus too little SWDS, leading to the cold Tsfc bias over the oceans that is largest in summer. All four simulations simulate too little cloud impact over land, but this bias is largest in the RASM_atm/RASM_atm_ice simulations, resulting in the large warm bias over land in summer.

The RASM_atm/RASM_atm_ice simulations differ from the RASM_ctrl/RASM1.0 simulations in their use

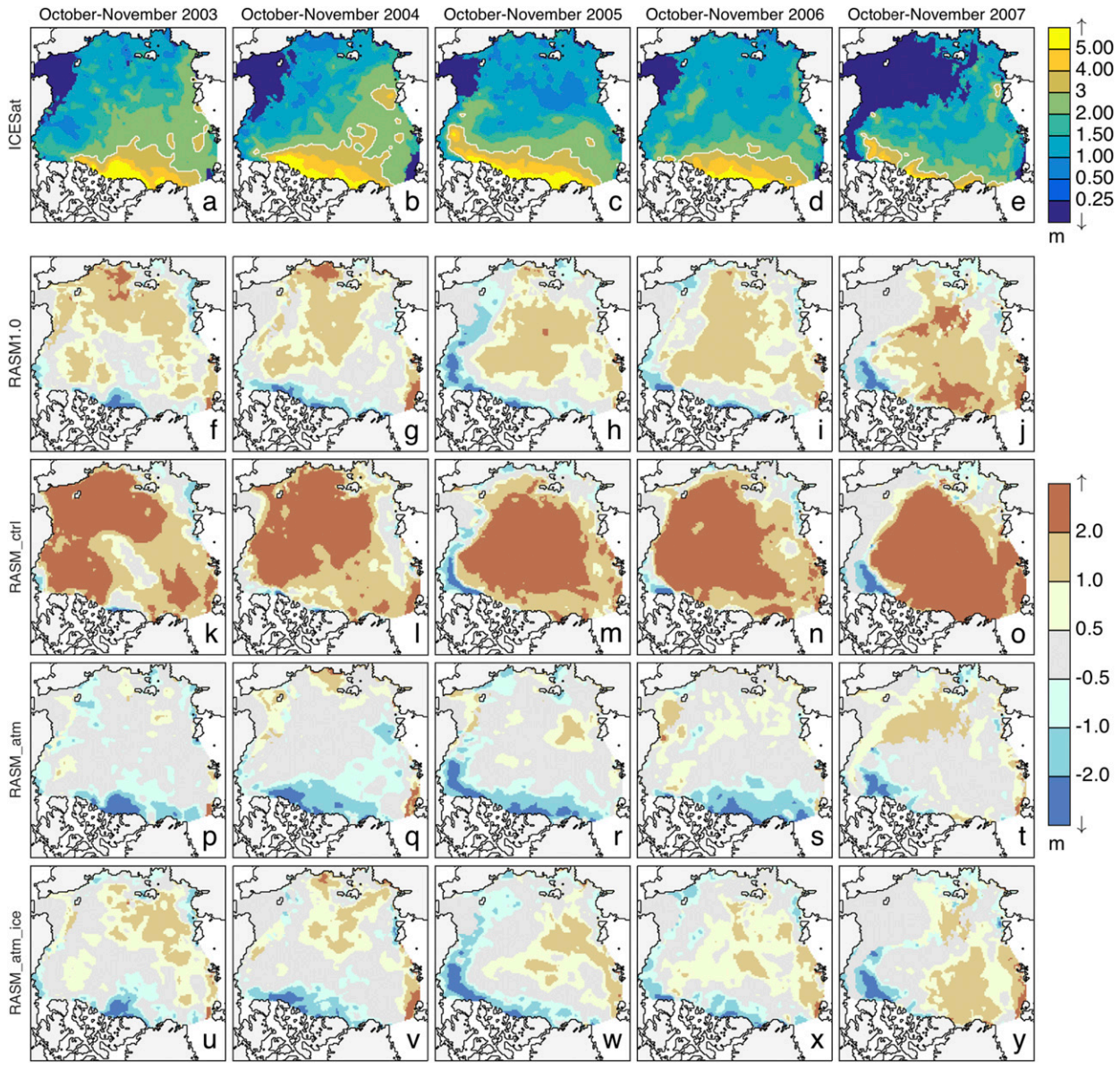

FIG. 12. (a)–(e) Fall (October–November) sea ice thickness estimated from ICESat, and mean deviation from Kwok and Cunningham (2008) for (f)–(j) RASM1.0, (k)–(o) RASM_ctrl, (p)–(t) RASM_atm, and (u)–(y) RASM_atm_ice.

of the MYNN instead of YSU boundary layer parameterization and the Kain–Fritsch instead of the Grell–Devenyi convective parameterization. These physics changes were motivated by results in Jousse et al. (2016) that showed that changes in WRF boundary layer and convective parameterizations resulted in more realistic simulation of boundary layer depth and cloud water path over the ocean. In the RASM_atm/RASM_atm_ice simulations, the change in WRF boundary layer and convective parameterizations reduced the radiation, temperature, and precipitation biases over the North Pacific in RASM (Fig. 7) and also result in a larger fraction of the modeled precipitation being generated by the convective parameterization in the RASM_atm/RASM_atm_ice simulations (Fig. 14). Since cloud variables were not saved as output in the RASM simulations presented in this paper, we cannot determine if changes in boundary layer depth and cloud water path, similar to those in Jousse et al. (2016), occur in RASM, but the change in radiative fluxes seen in RASM is consistent with the changes described in Jousse et al. (2016). While these WRF physics changes significantly improved the RASM simulations over the oceanic portions of the model domain, these same changes

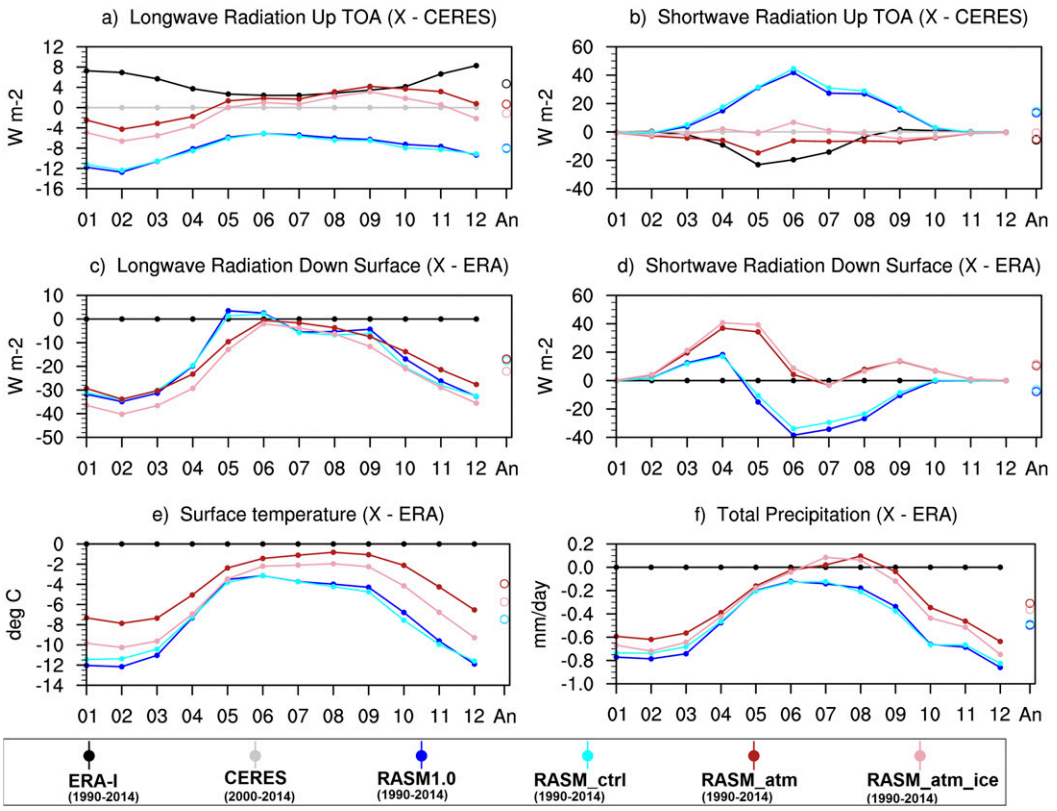

FIG. 13. As in Fig. 7, but for the subpolar Atlantic analysis domain shown in Fig. 1.

degraded the simulations over land and may reflect failures in this combination of boundary layer and convective parameterizations to capture the different boundary layer and convective cloud processes acting over land, especially in summer.

As noted above, the radiative impact of convective clouds is not accounted for in the WRF version used in RASM. As a result, the increase in convective cloud, as indicated by the increase in convective precipitation fraction (Fig. 14), along with the lack of radiative impact from convective clouds in WRF contributes to the positive SWDS bias seen in the RASM_atm/RASM_atm_ice simulations over land (Figs. 6 and 8) and the North Pacific (Figs. 6 and 7), but likely has little impact in the central Arctic where almost no convective clouds occur (Fig. 14). The next generation of RASM will use a newer version of WRF that simulates the radiative impact of convective clouds and should help reduce the positive SWDS bias seen in the current version of RASM.

The cold Tsfc bias in the Arctic and adjacent land areas in winter is related to a negative LWDS bias in all four RASM simulations (Fig. 5). The negative LWDS bias may be caused by RASM simulating too few or too optically thin clouds. We suspect that RASM is simulating too little supercooled cloud water in the cold winter clouds (Klein et al. 2009; Cesana et al. 2012), resulting in clouds that are too optically thin, which in turn results in a negative LWDS bias. Unfortunately, this cannot be assessed directly with these RASM simulations as cloud fields were not saved as part of the RASM output. Ongoing work to evaluate additional WRF physics parameterizations will save cloud fields for analysis and will use surface and satellite-based cloud remote sensing observations of cloud phase to assess this hypothesis.

Differences in the Tsfc biases for the four RASM simulations (Fig. 3) contribute to differences in the precipitation biases (Fig. 4) through changes in evaporation. All four RASM simulations evaluated in this paper use identical lateral boundary conditions and thus the atmospheric moisture flux across the boundaries is identical in these four simulations. Since the RASM_atm/RASM_atm_ice simulations generate more precipitation than the RASM_ctrl/RASM1.0 simulations (Fig. 4), this change in precipitation must be driven by an additional moisture source within the model domain. The RASM_ctrl/RASM1.0 simulations with cold Tsfc biases over the Pacific and Atlantic Oceans (Fig. 3) result in

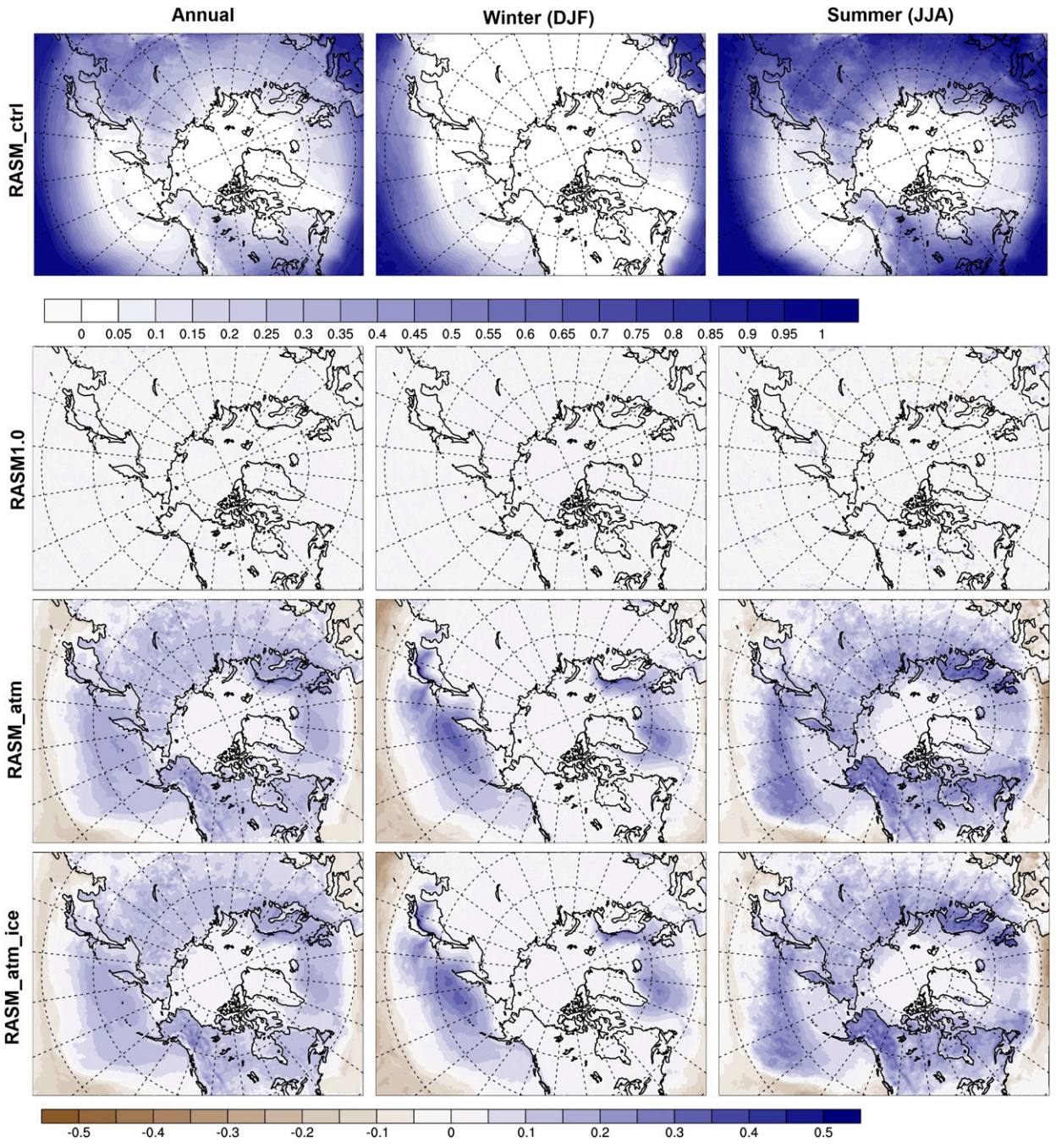

FIG. 14. (top) Fraction of total (left) annual, (middle) DJF, and (right) JJA precipitation generated by the WRF convective parameterization for the RASM_ctrl simulation. Also shown are differences between the RASM_ctrl fraction of total precipitation generated by the WRF convective parameterization and (second row) RASM_1.0, (third row) RASM_atm, and (bottom) RASM_atm_ice.

reduced evaporation within the model domain and an overall dry bias while the warmer RASM_atm/RASM_atm_ice simulations have more evaporation and near-zero or slightly positive precipitation biases (Fig. 4).

The suite of four RASM simulations presented in this paper show the large sensitivity of the simulated surface climate to changes in atmospheric model physics. In particular, the large changes in radiative fluxes, driven by changes in simulated cloud, between the RASM_ctrl/RASM1.0 and RASM_atm/RASM_atm_ice simulations lead to large differences in Tsfc and precipitation biases in these pairs of simulations. The simulated sea ice state also responds strongly to these changes in atmospheric physics (Figs. 10–12). The RASM_atm/RASM_atm_ice

simulations have less sea ice than the RASM_ctrl/RASM1.0 simulations, consistent with the domainwide increase in SWDS. The atmospheric state shows little sensitivity to the changes in ocean and sea ice parameters between the RASM_ctrl and RASM1.0 simulations, although slightly less sea ice is simulated in the RASM1.0 simulation. Other than Tsfc in the Arctic there is also little sensitivity of the atmospheric state to changes in sea ice physics between the RASM_atm and RASM_atm_ice pair of simulations, although sea ice thickness does respond to the sea ice physics changes in this pair of RASM simulations. Part of the lack of atmospheric sensitivity to changes in ocean and ice model options may be caused by the use of spectral nudging in WRF, but the fact that the atmospheric state does respond in significant ways to the changes in atmospheric physics suggests that the WRF nudging is not overly constraining the simulated atmospheric state. In terms of sea ice state, ocean temperature, and domainwide precipitation the RASM_atm_ice simulation is the best RASM simulation evaluated here, while the RASM1.0 simulation produces the most accurate surface climate over land areas.

The results described above highlight the critical role that clouds and radiation play in coupled climate system simulations. The RASM radiation errors described above have been attributed to errors in simulated clouds in RASM, although lack of cloud output from these simulations prevents a direct assessment of this statement. The radiation errors lead to errors in Tsfc, which over the ocean alters evaporation within the model domain and impacts domainwide precipitation. Changes in precipitation can further impact other aspects of the simulated climate system including sea ice growth or melt through changes in snow cover on the sea ice or changes in land surface state through changes in timing and thickness of snow cover or soil moisture. These changes in domainwide precipitation, and their additional impacts on other portions of the climate system, occur despite the constraints imposed on regional simulations by their lateral boundary conditions and/or nudging toward reanalysis fields. This also highlights the important role that midlatitude ocean areas play in mid- and high-latitude precipitation through evaporation driven by Tsfc in the actual climate system.

While the current version of RASM is able to produce reasonable simulations of Arctic and adjacent lower-latitude climate there are still some significant biases related to errors in cloud cover and radiative fluxes. Some of these errors are related to the fact that the version of WRF used in RASM does not account for the radiative impact of convective clouds but other errors are related to under or overestimation of cloud amount and/or optical thickness. We are currently assessing different cloud microphysics options in WRF and RASM and are upgrading RASM to use WRF v3.7, which will allow the radiative impact of convective clouds to be simulated, as well as including bug fixes and additional physics options. A more physically based assessment of RASM biases in these simulations will be conducted in the future that will expand upon the initial RASM results presented here. In particular, additional attention will be given to cloud amount and cloud phase in the future analysis and will rely on satellite observations of cloud properties.

Acknowledgments. This work was funded by the United States Department of Energy Grants DE-FG02-07ER64462 and DE-SC0006178 (University of Colorado), DE-FG02-07ER64460 and DE-SC0006856 (University of Washington), DE-FG02-07ER64463 (Iowa State University), DE-SC0006693 (University of Arizona) and National Science Foundation Grants PLR-1107788 and PLR-1417818 (University of Colorado). Computing resources were provided via a Challenge Grant from the U.S. Department of Defense as part of the High Performance Computing Modernization Program (HPCMP). Observationally based data used in this study were supplied by the U.S. National Snow and Ice Data Center, the European Centre for Medium-Range Weather Forecasts, the National Center for Atmospheric Research, and the Jet Propulsion Laboratory of the National Aeronautics and Space Administration. ERA-Interim data were accessed from the Research Data Archive at the National Center for Atmospheric Research, Computational and Information Systems Laboratory. RASM data are archived at the DoD-HPCMP center. We thank the four anonymous reviewers and the editor for their time and useful comments which helped improve this manuscript.

REFERENCES

Bennartz, R., and Coauthors, 2013: July 2012 Greenland melt extent enhanced by low-level liquid clouds. *Nature*, **496**, 83–86, doi:10.1038/nature12002.

Berg, P., R. Döscher, and T. Koenigk, 2013: Impacts of using spectral nudging on regional climate model RCA4 simulations of the Arctic. *Geosci. Model Dev.*, **6**, 849–859, doi:10.5194/gmd-6-849-2013.

Bi, D., and Coauthors, 2013: The ACCESS coupled model: Description, control climate and evaluation. *Aust. Meteor. Ocean J.*, **63**, 41–64, doi:10.22499/2.6301.004.

Bitz, C. M., and W. H. Lipscomb, 1999: An energy-conserving thermodynamic model of sea ice. *J. Geophys. Res.*, **104**, 15 669–15 677, doi:10.1029/1999JC900100.

Blanchard-Wrigglesworth, E., and C. M. Bitz, 2014: Characteristics of Arctic sea-ice thickness variability in GCMs. *J. Climate*, **27**, 8244–8258, doi:10.1175/JCLI-D-14-00345.1.

Bowling, L. C., and Coauthors, 2003: Simulation of high-latitude hydrological processes in the Torne–Kalix basin: PILPS Phase 2(e). *Global Planet. Change*, **38**, 1–30, doi:10.1016/S0921-8181(03)00003-1.

——, J. W. Pomeroy, and D. P. Lettenmaier, 2004: Parameterization of blowing-snow sublimation in a macroscale hydrology model. *J. Hydrometeor.*, **5**, 745–762, doi:10.1175/1525-7541(2004)005<0745:POBSIA>2.0.CO;2.

Bromwich, D. H., K. M. Hines, and L.-S. Bai, 2009: Development and testing of Polar Weather Research and Forecasting model: 2. Arctic Ocean. *J. Geophys. Res.*, **114**, D08122, doi:10.1029/2008JD010300.

——, A. B. Wilson, L.-S. Bai, G. W. K. Moore, and P. Bauer, 2016: A comparison of the regional Arctic System Reanalysis and the global ERA-Interim reanalysis for the Arctic. *Quart. J. Roy. Meteor. Soc.*, **142**, 644–658, doi:10.1002/qj.2527.

Cassano, J. J., M. Higgins, and M. Seefeldt, 2011: Performance of the Weather Research and Forecasting (WRF) model for month-long pan-Arctic simulations. *Mon. Wea. Rev.*, **139**, 3469–3488, doi:10.1175/MWR-D-10-05065.1.

Cesana, G., J. E. Kay, H. Chepfer, J. M. English, and G. de Boer, 2012: Ubiquitous low-level liquid-containing Arctic clouds: New observations and climate model constraints from CALIPSO-GOCCP. *Geophys. Res. Lett.*, **39**, L20804, doi:10.1029/2012GL053385.

Cherkauer, K. A., L. C. Bowling, and D. P. Lettenmaier, 2003: Variable infiltration capacity cold land process model updates. *Global Planet. Change*, **38**, 151–159, doi:10.1016/S0921-8181(03)00025-0.

Collins, W. D., and Coauthors, 2004: Description of the NCAR Community Atmosphere Model (CAM 3.0). NCAR Tech. Note NCAR/TN-464+STR, 226 pp. [Available online at http://www.cesm.ucar.edu/models/atm-cam/docs/description/description.pdf.]

Craig, A. P., M. Vertenstein, and R. Jacob, 2012: A new flexible coupler for Earth system modeling developed for CCSM4 and CESM1. *Int. J. High Perform. Comput.*, **26**, 31–42, doi:10.1177/1094342011428141.

Dee, D. P., and Coauthors, 2011: The ERA-Interim reanalysis: Configuration and performance of the data assimilation system. *Quart. J. Roy. Meteor. Soc.*, **137**, 553–597, doi:10.1002/qj.828.

Dorn, W., K. Dethloff, A. Rinke, S. Frickenhaus, R. Gerdes, M. Karcher, and F. Kauker, 2007: Sensitivities and uncertainties in a coupled regional atmosphere–ocean–ice model with respect to the simulation of Arctic sea ice. *J. Geophys. Res.*, **112**, D10118, doi:10.1029/2006JD007814.

——, ——, and ——, 2009: Improved simulation of feedbacks between atmosphere and sea ice over the Arctic Ocean in a coupled regional climate model. *Ocean Modell.*, **29**, 103–114, doi:10.1016/j.ocemod.2009.03.010.

——, ——, and ——, 2012: Limitations of a coupled regional climate model in the reproduction of the observed Arctic sea-ice retreat. *Cryosphere*, **6**, 985–998, doi:10.5194/tc-6-985-2012.

Döscher, R., and T. Koenigk, 2013: Arctic rapid sea ice loss events in regional coupled climate scenario experiments. *Ocean Sci.*, **9**, 217–248, doi:10.5194/os-9-217-2013.

——, U. Willén, C. G. Jones, A. Rutgersson, H. E. M. Meier, U. Hansson, and L. P. Graham, 2002: The development of the regional coupled ocean–atmosphere model RCAO. *Boreal Environ. Res.*, **7**, 183–192.

——, K. Wyser, H. E. M. Meier, M. Qian, and R. Redler, 2010: Quantifying Arctic contributions to climate predictability in a regional coupled ocean–ice–atmosphere model. *Climate Dyn.*, **34**, 1157–1176, doi:10.1007/s00382-009-0567-y.

Dukowicz, J. K., and R. D. Smith, 1994: Implicit free-surface method for the Bryan–Cox–Semtner ocean model. *J. Geophys. Res.*, **99**, 7991–8014, doi:10.1029/93JC03455.

DuVivier, A. K., and J. J. Cassano, 2013: Evaluation of WRF model resolution on simulated mesoscale winds and surface fluxes near Greenland. *Mon. Wea. Rev.*, **141**, 941–963, doi:10.1175/MWR-D-12-00091.1.

Dyer, A. J., and B. B. Hicks, 1970: Flux-gradient relationships in the constant flux layer. *Quart. J. Roy. Meteor. Soc.*, **96**, 715–721, doi:10.1002/qj.49709641012.

ECMWF, 2009: ERA-Interim Project. Research Data Archive at the National Center for Atmospheric Research, Computational and Information Systems Laboratory, accessed 1 August 2014, doi:10.5065/D6CR5RD9.

Flato, G., and Coauthors, 2013: Evaluation of climate models. *Climate Change 2013: The Physical Science Basis*, T. F. Stocker et al., Eds., Cambridge University Press, 741–866. [Available online at http://www.ipcc.ch/report/ar5/wg1/.]

Gent, P. R., and Coauthors, 2011: The Community Climate System Model version 4. *J. Climate*, **24**, 4973–4991, doi:10.1175/2011JCLI4083.1.

Giorgi, F., 1995: Perspectives for regional Earth system modeling. *Global Planet. Change*, **10**, 23–42, doi:10.1016/0921-8181(94)00018-9.

——, 2005: Interdecadal variability of regional climate change: Implications for the development of regional climate change scenarios. *Meteor. Atmos. Phys.*, **89**, 1–15, doi:10.1007/s00703-005-0118-y.

——, 2006: Regional climate modeling: Status and perspectives. *J. Phys. IV*, **139**, 101–118, doi:10.1051/jp4:2006139008.

——, and X. Bi, 2000: A study of internal variability of a regional climate model. *J. Geophys. Res.*, **105**, 29 503–29 521, doi:10.1029/2000JD900269.

——, and W. J. Gutowski Jr., 2015: Regional dynamical downscaling and the CORDEX initiative. *Annu. Rev. Environ. Resour.*, **40**, 467–490, doi:10.1146/annurev-environ-102014-021217.

Grell, G. A., and D. Devenyi, 2002: A generalized approach to parameterizing convection combining ensemble and data assimilation techniques. *Geophys. Res. Lett.*, **29**, 1693, doi:10.1029/2002GL015311.

Hamman, J. B., and Coauthors, 2016: Land surface climate in the Regional Arctic System Model. *J. Climate*, **29**, 6543–6562, doi:10.1175/JCLI-D-15-0415.1.

Hines, K. M., and D. H. Bromwich, 2008: Development and testing of Polar Weather Research and Forecasting (WRF) Model. Part I: Greenland ice sheet meteorology. *Mon. Wea. Rev.*, **136**, 1971–1989, doi:10.1175/2007MWR2112.1.

——, ——, L.-S. Bai, M. Barlage, and A. G. Slater, 2011: Development and testing of Polar WRF. Part III: Arctic land. *J. Climate*, **24**, 26–48, doi:10.1175/2010JCLI3460.1.

Hong, S.-Y., Y. Noh, and J. Dudhia, 2006: A new vertical diffusion package with an explicit treatment of entrainment processes. *Mon. Wea. Rev.*, **134**, 2318–2341, doi:10.1175/MWR3199.1.

Hunke, E. C., D. A. Hebert, and O. Lecomte, 2013: Level-ice melt ponds in the Los Alamos sea ice model, CICE. *Ocean Modell.*, **71**, 26–42, doi:10.1016/j.ocemod.2012.11.008.

——, W. H. Lipscomb, A. K. Turner, N. Jeffery, and S. Elliott, 2015: CICE: The Los Alamos Sea Ice Model documentation and software user's manual version 5.1. Los Alamos National Laboratory Rep. LA-CC-012, 114 pp.

Hurrell, J. W., and Coauthors, 2013: The Community Earth System Model: A framework for collaborative research. *Bull. Amer. Meteor. Soc.*, **94**, 1339–1360, doi:10.1175/BAMS-D-12-00121.1.

Iacono, M. J., J. S. Delamere, E. J. Mlawer, M. W. Shephard, S. A. Clough, and W. D. Collins, 2008: Radiative forcing by

long-lived greenhouse gases: Calculations with the AER radiative transfer models. *J. Geophys. Res.*, **113**, D13103, doi:10.1029/2008JD009944.

Jousse, A., A. Hall, F. Sun, and J. Teixeira, 2016: Causes of WRF energy fluxes biases in a stratocumulus region. *Climate Dyn.*, **46**, 571–584, doi:10.1007/s00382-015-2599-9.

Kain, J. S., 2004: The Kain–Fritsch convective parameterization: An update. *J. Appl. Meteor.*, **43**, 170–181, doi:10.1175/1520-0450(2004)043<0170:TKCPAU>2.0.CO;2.

Karlsson, J., and G. Svensson, 2013: Consequences of poor representation of Arctic sea-ice albedo and cloud-radiation interactions in the CMIP5 model ensemble. *Geophys. Res. Lett.*, **40**, 4374–4379, doi:10.1002/grl.50768.

Klaus, D., W. Dorn, K. Dethloff, A. Rinke, and M. Mielke, 2012: Evaluation of two cloud parameterizations and their possible adaptation to Arctic climate conditions. *Atmosphere*, **3**, 419–450, doi:10.3390/atmos3030419.

Klehmet, K., B. Geyer, and B. Rockel, 2013: A regional climate model hindcast for Siberia: Analysis of snow water equivalent. *Cryosphere*, **7**, 1017–1034, doi:10.5194/tc-7-1017-2013.

Klein, S. A., and Coauthors, 2009: Intercomparison of model simulations of mixed-phase clouds observed during the ARM Mixed-Phase Arctic Cloud Experiment. I: Single-layer cloud. *Quart. J. Roy. Meteor. Soc.*, **135**, 979–1002, doi:10.1002/qj.416.

Koenigk, T., R. Döscher, and G. Nikulin, 2011: Arctic future scenario experiments with a coupled regional climate model. *Tellus*, **63A**, 69–86, doi:10.1111/j.1600-0870.2010.00474.x.

Kwok, R., and G. F. Cunningham, 2008: ICESat over Arctic sea ice: Estimation of snow depth and ice thickness. *J. Geophys. Res.*, **113**, C08010, doi:10.1029/2008JC004753.

——, and D. A. Rothrock, 2009: Decline in Arctic sea ice thickness from submarine and ICESat records: 1958–2008. *Geophys. Res. Lett.*, **36**, L15501, doi:10.1029/2009GL039035.

Large, W. G., and S. G. Yeager, 2009: The global climatology of an interannually varying air–sea flux data set. *Climate Dyn.*, **33**, 341–364, doi:10.1007/s00382-008-0441-3.

Liang, X., D. Lettenmaier, E. F. Wood, and S. J. Burges, 1994: A simple hydrologically based model of land surface water and energy fluxes for general circulation models. *J. Geophys. Res.*, **99**, 14 415–14 428, doi:10.1029/94JD00483.

——, E. F. Wood, and D. P. Lettenmaier, 1996: Surface soil moisture parameterization of the VIC-2L model: Evaluation and modification. *Global Planet. Change*, **13**, 195–206, doi:10.1016/0921-8181(95)00046-1.

Lindsay, R., M. Wensnahan, A. Schweiger, and J. Zhang, 2014: Evaluation of seven different atmospheric reanalysis products in the Arctic. *J. Climate*, **27**, 2588–2606, doi:10.1175/JCLI-D-13-00014.1.

Loeb, N. G., B. A. Wielicki, D. R. Doelling, G. L. Smith, D. F. Keyes, S. Kato, N. Manalo-Smith, and T. Wong, 2009: Toward optimal closure of the earth's top-of-atmosphere radiation budget. *J. Climate*, **22**, 748–766, doi:10.1175/2008JCLI2637.1.

Lohmann, D., R. Nolte-Holube, and E. Raschke, 1996: A large-scale horizontal routing model to be coupled to land surface parameterization schemes. *Tellus*, **48A**, 708–721, doi:10.3402/tellusa.v48i5.12200.

Lynch, A. H., W. Chapman, J. E. Walsh, and G. Weller, 1995: Development of a regional climate model of the western Arctic. *J. Climate*, **8**, 1555–1570, doi:10.1175/1520-0442(1995)008<1555:DOARCM>2.0.CO;2.

Maslowski, W., D. Marble, W. Walczowski, U. Schauer, J. L. Clement, and A. J. Semtner, 2004: On climatological mass, heat, and salt transports through the Barents Sea and Fram Strait from a pan-Arctic coupled ice-ocean model simulation. *J. Geophys. Res.*, **109**, C03032, doi:10.1029/2001JC001039.

——, J. Clement Kinney, M. Higgins, and A. Roberts, 2012: The future of Arctic sea ice. *Annu. Rev. Earth Planet. Sci.*, **40**, 625–654, doi:10.1146/annurev-earth-042711-105345.

Maurer, E. P., A. W. Wood, J. C. Adam, D. P. Lettenmaier, and B. Nijssen, 2002: A long-term hydrologically based dataset of land surface fluxes and states for the conterminous United States. *J. Climate*, **15**, 3237–3251, doi:10.1175/1520-0442(2002)015<3237:ALTHBD>2.0.CO;2.

Meier, W. N., G. Peng, D. J. Scott, and M. H. Savoie, 2014: Verification of a new NOAA/NSIDC passive microwave sea-ice concentration climate record. *Polar Res.*, **33**, 21004, doi:10.3402/polar.v33.21004.

Miller, N. B., M. D. Shupe, C. J. Cox, V. P. Walden, D. D. Turner, and K. Steffen, 2015: Cloud radiative forcing at Summit, Greenland. *J. Climate*, **28**, 6267–6280, doi:10.1175/JCLI-D-15-0076.1.

Morrison, H., G. Thompson, and V. Tatarskii, 2009: Impact of cloud microphysics on the development of trailing stratiform precipitation in a simulated squall line: Comparison of one- and two-moment schemes. *Mon. Wea. Rev.*, **137**, 991–1007, doi:10.1175/2008MWR2556.1.

Nakanishi, M., and H. Niino, 2006: An improved Mellor–Yamada level-3 model: Its numerical stability and application to a regional prediction of advection fog. *Bound.-Layer Meteor.*, **119**, 397–407, doi:10.1007/s10546-005-9030-8.

Nijssen, B., D. P. Lettenmaier, X. Liang, S. W. Wetzel, and E. F. Wood, 1997: Streamflow simulation for continental-scale river basins. *Water Resour. Res.*, **33**, 711–724, doi:10.1029/96WR03517.

Paulson, C. A., 1970: The mathematical representation of wind speed and temperature profiles in the unstable atmospheric surface layer. *J. Appl. Meteor.*, **9**, 857–861, doi:10.1175/1520-0450(1970)009<0857:TMROWS>2.0.CO;2.

Porter, D. F., J. J. Cassano, and M. C. Serreze, 2011: Analysis of the Arctic atmospheric energy budget in WRF: A comparison with reanalyses and satellite observations. *J. Geophys. Res.*, **116**, D22108, doi:10.1029/2011JD016622.

Rind, D., 2008: The consequences of not knowing low- and high-latitude climate sensitivity. *Bull. Amer. Meteor. Soc.*, **89**, 855–864, doi:10.1175/2007BAMS2520.1.

Rinke, A., and K. Dethloff, 2000: On the sensitivity of a regional Arctic climate model to initial and boundary conditions. *Climate Res.*, **14**, 101–113, doi:10.3354/cr014101.

Roberts, A., J. J. Cassano, R. Doscher, L. Hinzman, M. M. Holland, H. Mitsudera, A. Sumi, and J. E. Walsh, 2010: A science plan for regional Arctic system modeling: A report by the Arctic Research Community for the National Science Foundation Office of Polar Programs. University of Alaska Fairbanks International Arctic Research Center Tech. Paper 10-0001, 49 pp. [Available online at www.iarc.uaf.edu/publications/reports/IARCTP10-0001.pdf.]

——, J. Cherry, R. Döscher, S. Elliott, and L. Sushama, 2011: Exploring the potential for Arctic system modeling. *Bull. Amer. Meteor. Soc.*, **92**, 203–206, doi:10.1175/2010BAMS2959.1.

——, and Coauthors, 2015: Simulating transient ice–ocean Ekman transport in the Regional Arctic System Model and Community Earth System Model. *Ann. Glaciol.*, **56**, 211–228, doi:10.3189/2015AoG69A760.

Saha, S., and Coauthors, 2010: The NCEP Climate Forecast System Reanalysis. *Bull. Amer. Meteor. Soc.*, **91**, 1015–1057, doi:10.1175/2010BAMS3001.1.

Samuelsson, P., and Coauthors, 2011: The Rossby Centre Regional Climate model RCA3: Model description and performance. *Tellus*, **63A**, 4–23, doi:10.1111/j.1600-0870.2010.00478.x.

Scinocca, J. F., and Coauthors, 2016: Coordinated global and regional climate modelling. *J. Climate*, **29**, 17–35, doi:10.1175/JCLI-D-15-0161.1.

Shupe, M. D., and J. M. Intrieri, 2004: Cloud radiative forcing of the Arctic surface: The influence of cloud properties, surface albedo, and solar zenith angle. *J. Climate*, **17**, 616–628, doi:10.1175/1520-0442(2004)017<0616:CRFOTA>2.0.CO;2.

Simmonds, I., 2015: Comparing and contrasting the behaviour of Arctic and Antarctic sea ice over the 35 year period 1979–2013. *Ann. Glaciol.*, **56**, 18–28, doi:10.3189/2015AoG69A909.

Skamarock, W. C., and Coauthors, 2008: A description of the Advanced Research WRF version 3. NCAR Tech. Note NCAR/TN-475+STR, 113 pp., doi:10.5065/D68S4MVH.

Smith, R. D., J. K. Dukowicz, and R. C. Malone, 1992: Parallel ocean circulation modeling. *Physica D*, **60**, 38–61, doi:10.1016/0167-2789(92)90225-C.

——, and Coauthors, 2010: The Parallel Ocean Program (POP) Reference Manual Ocean Component of the Community Climate System Model (CCSM) and Community Earth System Model (CESM). Rep. LAUR-01853, 141 pp. [Available online at https://ccsm.ucar.edu/models/cesm1.2/pop2/doc/sci/POPRefManual.pdf.]

Steele, M., R. Morley, and W. Ermold, 2001: PHC: A global ocean hydrography with a high-quality Arctic Ocean. *J. Climate*, **14**, 2079–2087, doi:10.1175/1520-0442(2001)014<2079:PAGOHW>2.0.CO;2.

Steiner, N., and Coauthors, 2015: Observed trends and climate projections affecting marine ecosystems in the Canadian Arctic. *Environ. Rev.*, **23**, 191–239, doi:10.1139/er-2014-0066.

Stroeve, J. C., V. Kattsov, A. Barrett, M. Serreze, T. Pavlova, M. Holland, and W. N. Meier, 2012: Trends in Arctic sea ice extent from CMIP5, CMIP3 and observations. *Geophys. Res. Lett.*, **39**, L16502, doi:10.1029/2012GL052676.

Taylor, K. E., R. J. Stouffer, and G. A. Meehl, 2012: An overview of CMIP5 and the experiment design. *Bull. Amer. Meteor. Soc.*, **93**, 485–498, doi:10.1175/BAMS-D-11-00094.1.

Tilling, R. L., A. Ridout, A. Shepherd, and D. J. Wingham, 2015: Increased Arctic sea ice volume after anomalously low melting in 2013. *Nat. Geosci.*, **8**, 643–646, doi:10.1038/ngeo2489.

Tsamados, M., D. L. Feltham, and A. V. Wilchinsky, 2013: Impact of a new anisotropic rheology on simulations of Arctic sea ice. *J. Geophys. Res. Oceans*, **118**, 91–107, doi:10.1029/2012JC007990.

Turner, A. K., and E. C. Hunke, 2015: Impacts of a mushy-layer thermodynamic approach in global sea-ice simulations using the CICE sea-ice model. *J. Geophys. Res. Oceans*, **120**, 1253–1275, doi:10.1002/2014JC010358.

——, ——, and C. M. Bitz, 2013: Two modes of sea-ice gravity drainage: A parameterization for large-scale modeling. *J. Geophys. Res. Oceans*, **118**, 2279–2294, doi:10.1002/jgrc.20171.

Urrego-Blanco, J. R., N. M. Urban, E. C. Hunke, A. K. Turner, and N. Jeffery, 2016: Uncertainty quantification and global sensitivity analysis of the Los Alamos sea ice model. *J. Geophys. Res. Oceans*, **121**, 2709–2732, doi:10.1002/2015JC011558.

von Storch, H., and F. W. Zwiers, 1999: *Statistical Analysis in Climate Research*. Cambridge University Press, 484 pp.

Webb, E. K., 1970: Profile relationships: The log-linear range, and extension to strong stability. *Quart. J. Roy. Meteor. Soc.*, **96**, 67–90, doi:10.1002/qj.49709640708.

Wielicki, B. A., B. R. Barkstrom, E. F. Harrison, R. B. Lee III, G. L. Smith, and J. E. Cooper, 1996: Clouds and the Earth's Radiant Energy System (CERES): An Earth Observing System Experiment. *Bull. Amer. Meteor. Soc.*, **77**, 853–868, doi:10.1175/1520-0477(1996)077<0853:CATERE>2.0.CO;2.

Wilks, D. S., 2006: *Statistical Methods in the Atmospheric Sciences*. 2nd ed. Academic Press, 627 pp.

Zappa, G., G. Masato, L. Shaffrey, T. Woollings, and K. Hodges, 2014: Linking Northern Hemisphere blocking and storm track biases in the CMIP5 climate models. *Geophys. Res. Lett.*, **41**, 135–139, doi:10.1002/2013GL058480.

Zhou, X., and Coauthors, 2014: Evaluation of Arctic land snow cover characteristics, surface albedo, and temperature during the transition seasons from regional climate model simulations and satellite data. *Adv. Meteor.*, **2014**, 604157, doi:10.1155/2014/604157.

Zhu, C., L. R. Leung, D. Gochis, Y. Qian, and D. P. Lettenmaier, 2009: Evaluating the influence of antecedent soil moisture on variability of the North American monsoon precipitation in the Coupled MM5/VIC Modeling System. *J. Adv. Model. Earth Syst.*, **1**, 13, doi:10.3894/JAMES.2009.1.13.